

Learning Rate Scaling across LoRA Ranks and Transfer to Full Finetuning

Nan Chen¹ Soledad Villar¹ Soufiane Hayou¹

Abstract

Low-Rank Adaptation (LoRA) is a standard tool for parameter-efficient finetuning of large models. While it induces a small memory footprint, its training dynamics can be surprisingly complex as they depend on several hyperparameters such as initialization, adapter rank, and learning rate. In particular, it is unclear *how the optimal learning rate scales with adapter rank*, which forces practitioners to re-tune the learning rate whenever the rank is changed. In this paper, we introduce *Maximal-Update Adaptation* (μ A), a theoretical framework that characterizes how the “optimal” learning rate should scale with model width and adapter rank to produce stable, non-vanishing feature updates under standard configurations. μ A is inspired from the Maximal-Update Parametrization (μ P) in pretraining. Our analysis leverages techniques from hyperparameter transfer and reveals that the optimal learning rate exhibits different scaling patterns depending on initialization and LoRA scaling factor. Specifically, we identify two regimes: one where the optimal learning rate remains roughly invariant across ranks, and another where it scales inversely with rank. We further identify a configuration that allows learning rate transfer from LoRA to full finetuning, drastically reducing the cost of learning rate tuning for full finetuning. Experiments across language, vision, vision–language, image generation, and reinforcement learning tasks validate our scaling rules and show that learning rates tuned on LoRA transfer reliably to full finetuning.

1. Introduction

The widespread availability of large pretrained models has made finetuning the standard approach to adapt a general-

¹Department of Applied Mathematics and Statistics, Johns Hopkins University, Maryland, United States of America.. Correspondence to: Soledad Villar <svillar3@jhu.edu>, Soufiane Hayou <hayou@jhu.edu>.

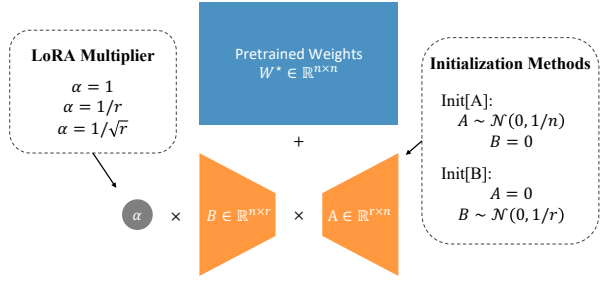


Figure 1. LoRA finetuning with standard design choices.

purpose model to a specific downstream task [65, 14]. At the same time, model capability typically improves with scale, with state-of-the-art language and vision models now reaching hundreds of billions of parameters [52, 83, 74]. The improvement in performance with scale makes larger models attractive to practitioners, but it also makes full finetuning (FFT) increasingly expensive. While FFT remains the standard for tasks such as instruction-tuning [3], parameter-efficient finetuning (PEFT) has become a default approach in many settings [22]. Low-Rank Adaptation (LoRA) [36] is arguably the most popular parameter-efficient finetuning method. It adds a low-rank factorization αBA to the (frozen) pretrained weight matrix $W^* \in \mathbb{R}^{n \times n}$, where $B \in \mathbb{R}^{n \times r}$, $A \in \mathbb{R}^{r \times n}$, r is the LoRA rank, and α is a scaling multiplier. Only B and A are trainable in this setting.

Deploying LoRA in practice requires several design choices beyond the rank r . To start from a no-op adapter, practitioners typically initialize one factor to random values and the other to zero; we denote these two common choices as Init[A] (random A , $B = 0$) and Init[B] (random B , $A = 0$) [27]. In addition, common implementations use different rank-dependent multipliers, typically $\alpha \in \{1, r^{-1}, r^{-1/2}\}$ [38, 3]; Figure 1 summarizes these standard choices. Because LoRA update is bilinear in A and B , the initialization, multiplier α , rank r , and learning rate η are coupled and jointly determine the effective update magnitude. This coupling makes hyperparameter tuning brittle in practice. Changing the rank or switching between initialization and multiplier choices can render a previously optimal learning rate suboptimal, forcing costly re-tuning. Figure 2 provides a representative example on Llama-3.2-1B finetuned on the Tulu3 dataset, showing end-

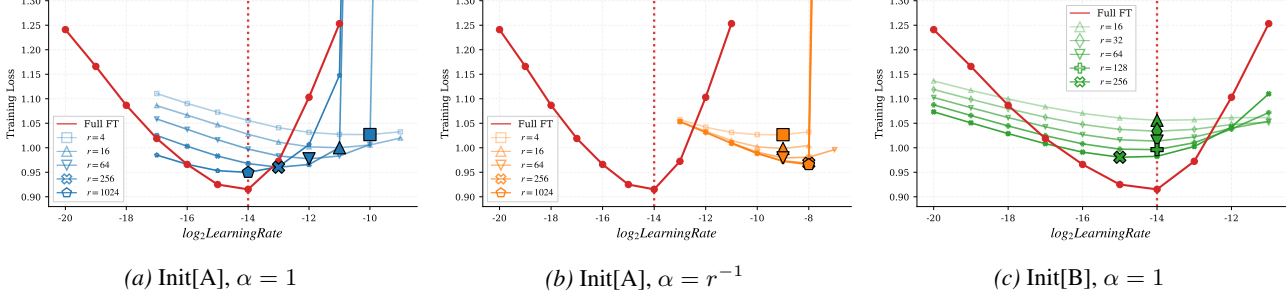


Figure 2. Learning rate sweeps for three standard LoRA configurations on Llama-3.2-1B (Tulu3). Each panel plots final training loss (EMA-smoothed) versus log-scale learning rate $\log_2(\eta)$ for multiple ranks (colored) and FFT (red). Large markers indicate the optimal learning rate for each rank; the dashed red line marks the optimal FFT learning rate. The y-axis is clipped for readability.

of-training loss as a function of learning rate for multiple ranks under three common configurations. Under Init[A] with constant $\alpha = 1$, the best learning rate decreases with rank r (Figure 2a). Setting $\alpha = r^{-1}$ while keeping Init[A] yields a different pattern: the optimal learning rate becomes approximately rank-invariant, but the stable range is narrow—small increases above the optimum cause divergence (Figure 2b). With Init[B] and constant $\alpha = 1$, the optimal learning rate is again rank-invariant and now aligns with the FFT optimum (Figure 2c). Notably, this optimal rate is more than an order of magnitude smaller than under Init[A] with $\alpha = r^{-1}$. Taken together, these experiments show that the learning rate–rank relationship changes qualitatively across initialization and multiplier choices. This raises a natural question: *how does the optimal learning rate η depend on rank r ?*

To answer this question, we analyze LoRA finetuning in the joint limit $n, r \rightarrow \infty$. Building on prior works analyzing infinite-width networks [84, 85, 27, 28], we study how initialization, multiplier α , and learning rate η jointly govern the magnitude of LoRA updates under a tractable theoretical setup. This allows us to characterize when LoRA updates remain bounded yet non-vanishing in the large- n , large- r regime—avoiding instability while ensuring learning does not stall. We call this regime the Maximal-Update Adaptation (μ A). From this analysis, we derive explicit scaling prescriptions for how the learning rate should depend on model width and LoRA rank under each configuration. These prescriptions explain why some configurations (e.g., Init[A] with constant α) require the learning rate to decrease with rank, while others (e.g., Init[B] with constant α) admit rank-invariant learning rates. Our analysis also connects LoRA to FFT. For Init[B] with constant α , the learning rate scaling that ensures stable feature learning matches that of FFT under the same assumptions. This matching is a necessary condition for hyperparameter transfer between the two regimes.

We verify our theory through extensive experiments spanning diverse tasks, modalities, and training paradigms.

Across all settings, the observed learning rate–rank patterns consistently match our derived scaling rules, confirming that μ A scaling rules generalize across architectures and domains. Our contributions are summarized as follows:

- We introduce μ A (Maximal-Update Adaptation), a theoretical framework for LoRA finetuning dynamics in the joint limit $n, r \rightarrow \infty$ and characterize how the optimal learning rate scales with model width and adapter rank to ensure maximal (stable) adaptation.
- Our analysis reveals two distinct regimes: one where the optimal learning rate scales inversely with rank, and one in which it remains rank-invariant. We identify a LoRA configuration where the optimal learning rate matches that of FFT (transfer from LoRA to FFT).
- Extensive experiments demonstrate that μ A scaling rules guarantee learning rate transfer across LoRA ranks and from LoRA and to FFT.

2. Related Works

Parameter-efficient finetuning. PEFT techniques fall into three main categories [22, 37]: (i) selectively updating a subset of parameters [9, 20, 50]; (ii) adding lightweight adapters [68, 35, 51, 31, 36]; or (iii) tuning continuous prompts [47, 44, 54]. LoRA [36] exemplifies the additive method and has inspired numerous variants targeting efficiency [77, 92, 13, 42, 39, 48, 53, 29] and stability [28, 27, 89]. Recent studies compare LoRA and FFT across gradient alignment [80, 81], expressive power [91], and spectral structure of weight updates [72]. Complementing these studies, we identify a LoRA configuration where the optimal learning rate matches that of FFT, guaranteeing learning rate transfer between the two methods.

Design choices of LoRA. Standard schemes randomly initialize either A or B using established techniques [17, 32], setting the other to zero. Alternative methods initialize

weights from pretrained weights [5, 58], deterministic orthogonal bases [93], downstream data [88, 62, 80], or quantized models [49]. Prior theoretical analyses of initialization [27, 46] focus on the infinite-width regime and treat the rank as constant; in contrast, we study the joint limit where both width n and rank r grow. For the LoRA multiplier α , the original LoRA [36] uses $\alpha = r^{-1}$ to keep update magnitudes controlled, rsLoRA [38] proposes $\alpha = r^{-1/2}$ for stability at larger ranks, and recent works increasingly adopt $\alpha = 1$ [16, 3, 7]. Schulman [70] empirically studies LoRA design choices but provides only heuristic rules for learning rate transfer between LoRA and FFT (e.g. dividing LoRA’s learning rate by 10 to obtain FFT’s learning rate). Another empirical work by Milsom et al. [59] introduced a general rule for learning rate transfer across LoRA ranks but did not provide any explanation to the observed scaling rules. None of these works provide a theoretical analysis of learning rate transfer with LoRA finetuning. In this paper, we propose a principled approach to learning rate transfer across LoRA ranks and from LoRA to FFT.

Asymptotic scaling analysis. Our analysis builds on prior works analyzing the asymptotic behavior of neural networks as width approaches infinity [84, 85, 86, 27, 28]. Related works apply similar frameworks to analyze depth scaling [25, 26, 30, 24, 61, 87]. Most closely related to ours are Hayou et al. [27, 28], which analyze LoRA finetuning in the limit $n \rightarrow \infty$ but treat the rank r as constant. This analysis does not reveal how training dynamics depend on the rank r . Here, we analyze the joint limit $n, r \rightarrow \infty$, yielding scaling prescriptions that depend on both network width and LoRA rank. Empirically, the optimal learning rate closely match derived scaling rules.

3. Setup and Definitions

We introduce definitions and notation for our theoretical analysis, following Hayou et al. [27].

3.1. LoRA Layer and Features

Definition 3.1 (Low-Rank Adaptation (LoRA)). Let $W^* \in \mathbb{R}^{n \times n}$ be a pretrained weight matrix that remains fixed during finetuning. LoRA parameterizes the weights as

$$W = W^* + \alpha B A,$$

where $B \in \mathbb{R}^{n \times r}$ and $A \in \mathbb{R}^{r \times n}$ are trainable factors with rank $r \ll n$ and $\alpha \in \mathbb{R}$ is a scalar multiplier.

For a generic LoRA-augmented linear layer, we denote the input by $\underline{Z} \in \mathbb{R}^n$ and the output by $\bar{Z} \in \mathbb{R}^n$,

$$\bar{Z} = W^* \underline{Z} + \alpha B A \underline{Z}.$$

LoRA factors are usually initialized with $B A = 0$ so that

finetuning starts from the pretrained model. There are two straightforward schemes that satisfy this property.

Definition 3.2 (Initialization schemes for LoRA). To initialize the LoRA update as a no-op, we consider:¹

- **Init[A]:** A_0 has i.i.d. entries $\mathcal{N}(0, 1/n)$ and $B_0 = 0$.
- **Init[B]:** B_0 has i.i.d. entries $\mathcal{N}(0, 1/r)$ and $A_0 = 0$.

We now define the intermediate and output LoRA features.

Definition 3.3 (LoRA features). For a layer input \underline{Z} , define the intermediate and output LoRA features

$$Z_A := A \underline{Z} \in \mathbb{R}^r, \quad Z_B := \alpha B Z_A = \alpha B A \underline{Z} \in \mathbb{R}^n.$$

We consider a fixed number T of finetuning steps, where T is independent of n and r . For $t \leq T$, we use superscripts to denote LoRA features at step t , i.e. Z_A^t, Z_B^t and subscripts to denote weights at step t , i.e. A_t, B_t .

To isolate the contribution of a single LoRA module to feature learning, we assume that only one LoRA layer is trainable while all other network components remain frozen. Under this assumption, the layer input \underline{Z} (corresponding to a given model input x) remains constant during finetuning.

At any step t , recall that $Z_A^t = A_t \underline{Z}$ and $Z_B^t = \alpha B_t Z_A^t$. Expanding the increment $\Delta Z_B^t := Z_B^t - Z_B^{t-1}$ yields:

$$\Delta Z_B^t = \underbrace{\alpha B_{t-1} \Delta Z_A^t}_{\delta_t^1} + \underbrace{\alpha \Delta B_t Z_A^{t-1}}_{\delta_t^2} + \underbrace{\alpha \Delta B_t \Delta Z_A^t}_{\delta_t^3} \quad (1)$$

We refer to the three contributions in Equation (1) as δ_t^1 , δ_t^2 , and δ_t^3 . As previously explained in Hayou et al. [28], the terms δ_t^1 and δ_t^2 correspond to *linear* updates in which one LoRA factor is trained while the other is held fixed, whereas δ_t^3 corresponds to the *multiplicative updates* of A and B . The next section discusses this decomposition and how it relates to stable feature learning.

3.2. Stable Feature Learning

We aim to understand how feature updates behave as a function of model width n and LoRA rank r . For this purpose, we consider the setting where both n and r grow, subject to $r \leq n$. To formalize how features and updates scale with (n, r) , we adopt the following asymptotic notation.

Definition 3.4 (Asymptotic notation). For sequences $c_{n,r} \in \mathbb{R}$ and $d_{n,r} \in \mathbb{R}_+$, we write $c_{n,r} = \mathcal{O}(d_{n,r})$ (resp. $c_{n,r} = \Omega(d_{n,r})$) if there exist constants $\kappa > 0$ and $N \in \mathbb{N}$ such that for all $n, r > N$ with $r \leq n$, we have $|c_{n,r}| < \kappa d_{n,r}$

¹The choice of the Gaussian distribution here is for simplification purpose only. It can be replaced with any centred distribution with finite second moment.

(resp. $|c_{n,r}| > \kappa d_{n,r}$). We write $c_{n,r} = \Theta(d_{n,r})$ if both bounds hold. This notation extends element-wise to vectors: for $c_{n,r} = (c_{n,r}^i)_{i=1}^k \in \mathbb{R}^k$ and $d_{n,r} = (d_{n,r}^i)_{i=1}^k \in \mathbb{R}_+^k$, we write $c_{n,r} = \mathcal{O}(d_{n,r})$ when $c_{n,r}^i = \mathcal{O}(d_{n,r}^i)$ for all $i \in [k]$, and similarly for Ω and Θ . For random variables, the notation is understood in the second-moment sense: $c_{n,r} = \mathcal{O}(d_{n,r})$ means $(\mathbb{E}|c_{n,r}|^2)^{1/2} = \mathcal{O}(d_{n,r})$.

Our stability objective requires that the LoRA-induced feature contribution Z_B^t remains bounded over T finetuning steps (where T is fixed), so that activations remain bounded.

Definition 3.5 (Feature stability). Fix a finite number of finetuning steps T independent of (n, r) . We say LoRA finetuning is *stable* if for all steps $t \leq T$, we have $Z_B^t = \mathcal{O}(1)$ in the joint limit $n, r \rightarrow \infty$ with $r \leq n$.

Since LoRA is typically initialized as a no-op ($Z_B^0 = 0$), Lemma 3.6 below implies that bounding the per-step increments $\Delta Z_B^t = \mathcal{O}(1)$ is sufficient for stability.

Lemma 3.6 (Telescoping bound). Fix $t \leq T$. If $Z_B^0 = \mathcal{O}(1)$ and $\Delta Z_B^s = \mathcal{O}(1)$ for all $s \leq t$, then $Z_B^t = \mathcal{O}(1)$.

However, stability alone permits trivial solutions—for instance, initializing both A and B to zero yields vanishing updates. We therefore require that the LoRA feature increment remains order-one.

Definition 3.7 (Stable feature learning with LoRA). We say LoRA induces *stable feature learning* if the dynamics are stable (Definition 3.5), and $\Delta Z_B^t = \Theta(1)$ for all $t \leq T$.

Intuitively, having $\Delta Z_B^t = \Theta(1)$ is associated with “maximal” adaptation in a similar fashion to μ P for pretraining, see [84]. By enforcing this condition, we derived *Maximal-Update Adaptation* scaling rules in the next section. Beyond stability, it is useful to understand *which* components of the update drive learning. Ideally, each of δ_t^1 , δ_t^2 , and δ_t^3 should be $\Theta(1)$, indicating that both factors A and B contribute meaningfully within each step. Accordingly, in our main results we track the term-wise scalings as a diagnostic: if a term vanishes in the large- (n, r) limit, the corresponding factor becomes effectively inactive.

Recall from Equation (1) that the feature update ΔZ_B^t decomposes into three terms $(\delta_t^i)_{i \in \{1,2,3\}}$. A sufficient condition for stability is to bound each term individually:

$$\delta_t^1 = \mathcal{O}(1), \quad \delta_t^2 = \mathcal{O}(1), \quad \delta_t^3 = \mathcal{O}(1).$$

This term-wise control avoids relying on cancellations among the three contributions. Stable feature learning additionally requires $\Delta Z_B^t = \Theta(1)$, which implies that at least one term must be $\Omega(1)$ under the chosen scaling, while the remaining terms may be lower-order.

4. Maximal-Update Adaptation (μ A)

We now state the learning rate scaling rules that guarantee stable feature learning under Init[A] and Init[B]. Full proofs and derivations (including the scaling of each δ_t^i) appear in Appendix A. Our analysis relies on two assumptions: (i) bounded forward and backward signals at each step, and (ii) a SignSGD update rule that uses the sign of the gradient, serving as a tractable proxy for the Adam optimizer.

Assumption 4.1 (Bounded forward/backward signals). For any fixed step $t \leq T$, the layer input and the backpropagated output gradient satisfy

$$Z = \Theta(1), \quad d\bar{Z} := \frac{\partial \mathcal{L}}{\partial \bar{Z}} = \Theta(1).$$

This ensures that features and gradients neither explode nor vanish at any step as $(n, r) \rightarrow \infty$.

Assumption 4.2 (Optimizer abstraction). We use a simplified variant of Adam [40] without momentum, reducing it to SignSGD [2], which gives element-wise sign updates:

$$g_A^t := \text{sign}\left(\frac{\partial \mathcal{L}_t}{\partial A_{t-1}}\right), \quad g_B^t := \text{sign}\left(\frac{\partial \mathcal{L}_t}{\partial B_{t-1}}\right),$$

and parameter updates

$$A_t = A_{t-1} - \eta g_A^t, \quad B_t = B_{t-1} - \eta g_B^t,$$

where $\text{sign}(\cdot)$ is applied element-wise (with $\text{sign}(0) = 0$) and η denotes the learning rate.

Following [27], we consider the setting where the loss is computed on a single sample. This simplifies the theoretical analysis and yields closed-form expressions. In what follows, we characterize the asymptotic behavior of feature updates as a function of (n, r) and show that it depends on initialization schemes. We present the results for Init[A] and Init[B] and compare the differences.

4.1. Init[A] Analysis

We begin with Init[A], where A_0 is randomly initialized and $B_0 = 0$. Theorem 4.3 characterizes the scale of the LoRA feature increment ΔZ_B^t . Corollary 4.4 then yields the learning rate scaling that achieves stable feature learning.

Theorem 4.3 (Init[A]). Under Assumptions 4.1 and 4.2, for any fixed $t \leq T$ with Init[A],

$$\Delta Z_B^t = \max\{\Theta(\eta\alpha r), \Theta(\eta^2\alpha rn)\}.$$

Imposing the stable feature learning condition $\Delta Z_B^t = \Theta(1)$ yields the following scaling rule for learning rate η .

Corollary 4.4 (μ A scaling rules for Init[A]). Let $\alpha = r^{-\gamma}$ for $\gamma \in [0, 1]$. Under Init[A], achieving stable feature learning (i.e., $\Delta Z_B^t = \Theta(1)$ for fixed $t \leq T$) requires

$$\eta = \Theta(n^{-1/2}r^{-(1-\gamma)/2}).$$

Table 1. μ A scaling rules from Corollary 4.4 for common choices of α . Each cell shows the argument of $\Theta(\cdot)$.

γ	α	η	Z_A^t
0	1	$n^{-1/2}r^{-1/2}$	$n^{1/2}r^{-1/2}$
$\frac{1}{2}$	$r^{-1/2}$	$n^{-1/2}r^{-1/4}$	$n^{1/2}r^{-1/4}$
1	r^{-1}	$n^{-1/2}$	$n^{1/2}$

With this choice,

$$\delta_t^1 = \Theta(r^{-1/2}), \delta_t^2 = \Theta(1), \delta_t^3 = \Theta(r^{-1/2}),$$

and the intermediate feature scales as

$$Z_A^t = \Theta(n^{1/2}r^{-(1-\gamma)/2}).$$

To make the prescriptions concrete, we summarize the resulting scalings for common multiplier choices in Table 1.

Interpretation of Corollary 4.4. We highlight the following key insights drawn from the corollary.

Learning rate scaling with rank. For a fixed model width n , the relationship between the optimal learning rate and rank r depends on the choice of α . With $\alpha = 1$, the learning rate decreases as $\eta \propto r^{-1/2}$: increasing the rank by $4\times$ requires halving the learning rate, consistent with Figure 2a. In contrast, setting $\alpha = r^{-1}$ absorbs the rank dependence, yielding a rank-invariant learning rate that depends only on width, consistent with Figure 2b.

Intermediate feature scaling. The intermediate features Z_A^t grow with width n but shrink with rank when $\alpha \in \{1, r^{-1/2}\}$. For $\alpha = 1$, doubling the rank reduces the intermediate feature scale by $\sqrt{2}$, which can improve internal numerical stability in wide models where large intermediate activations have been identified as a source of training instability [27]. However, when $\alpha = r^{-1}$, increasing the rank no longer suppresses the intermediate scale, which may explain why Init[A] with $\alpha = r^{-1}$ exhibits a narrower stable learning rate range in practice.

Learning efficiency. Under the stable learning rate scaling, only δ_t^2 remains order-one while δ_t^1 and δ_t^3 vanish as r grows. Since δ_t^1 captures the contribution of updating A , this means that changes to A contribute negligibly to the overall feature update. As a result, the adapter increasingly behaves like a random projection $Z_A \approx A_0 \mathcal{Z}$ with A held fixed at initialization, while learning proceeds primarily through B . This imbalance between the two factors is intrinsic to Init[A] and persists across all standard choices of α .

4.2. Init[B] Analysis

We next consider Init[B], where B_0 is randomly initialized and $A_0 = 0$.

Theorem 4.5 (Init[B]). *Under Assumptions 4.1 and 4.2, for any fixed $t \leq T$ with Init[B],*

$$\Delta Z_B^t = \max\{\Theta(\eta\alpha n), \Theta(\eta^2\alpha nr)\}.$$

Unlike Init[A], the resulting learning rate prescription depends more sensitively on how α scales with r . In the main text we focus on the most common configuration $\alpha = 1$ and defer additional cases to Appendix A.5.

Corollary 4.6 (μ A scaling rules for Init[B] with $\alpha = 1$). *Let $\alpha = 1$. Under Init[B], achieving stable feature learning (i.e., $\Delta Z_B^t = \Theta(1)$ for fixed $t \leq T$) requires*

$$\eta = \Theta(n^{-1}).$$

With this choice,

$$\delta_t^1 = \Theta(1), \delta_t^2 = \Theta(rn^{-1}), \delta_t^3 = \Theta(r^{1/2}n^{-1}),$$

and the intermediate feature scales as

$$Z_A^t = \Theta(1).$$

Interpretation of Corollary 4.6. This corollary reveals a regime qualitatively different from Init[A].

Rank-invariant learning rate. With $\alpha = 1$, the required learning rate scales only with width ($\eta \propto n^{-1}$) and is independent of rank. This explains the roughly rank-invariant optimal learning rate observed under Init[B] in Figure 2c.

Connection to FFT. The same width scaling $\eta \propto n^{-1}$ arises for full finetuning of a linear layer under the same SignSGD abstraction (see Theorem A.23 in Appendix A.6). This matching shows a necessary condition for learning rate transfer between LoRA and FFT: a learning rate tuned for Init[B] with $\alpha = 1$ can serve as a reasonable starting point for FFT without re-tuning. We empirically verify this transferability in our experiments.

Intermediate feature scaling. The intermediate features Z_A^t remain order-one throughout training, keeping internal activations controlled regardless of width.

Learning efficiency. The term-wise contributions exhibit the opposite imbalance from Init[A]: here $\delta_t^1 = \Theta(1)$ while δ_t^2 and δ_t^3 vanish when $r \ll n$. When the rank is much smaller than the width, updates to B contribute negligibly, and the adapter behaves as though B were fixed at its random initialization, with learning occurring primarily through A . Nonetheless, increasing the rank can strengthen δ_t^2 ; in the extreme case where r is on the order of n , both factors contribute meaningfully to feature updates.

5. Experiments

Our experiments verify μ A scaling rules empirically and learning rate transfer from LoRA to FFT. We examine three

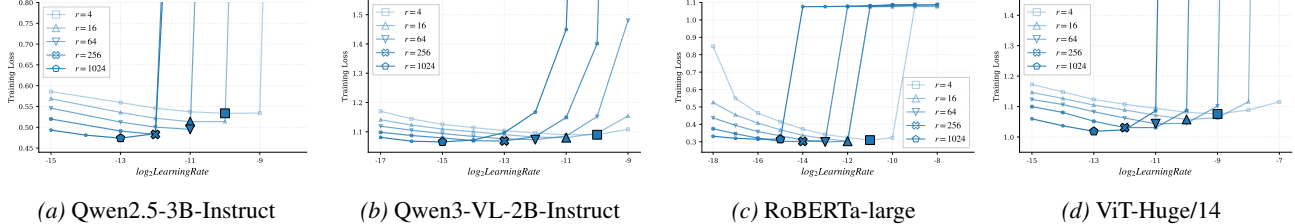


Figure 3. Learning rate sweeps for Init[A] with $\alpha = 1$ across four models. Curves show final training loss (EMA-smoothed) versus log-scale learning rate ($\log_2(\eta)$). Large markers denote per-rank optima. The Y-axis is clipped for readability.

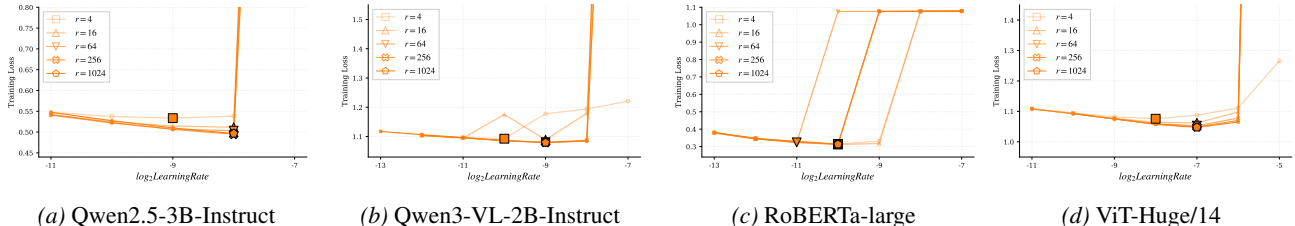


Figure 4. Learning rate sweeps for Init[A] with rank-dependent $\alpha = r^{-1}$ across four models. Curves show final training loss (EMA-smoothed) versus log-scale learning rate ($\log_2(\eta)$). Large markers denote per-rank optima. The Y-axis is clipped for readability.

regimes: supervised finetuning (SFT) across diverse architectures, reinforcement learning with verifiable rewards (RLVR), and text-to-image diffusion model finetuning.

5.1. Experimental Setup

Unified finetuning recipe. We use a unified finetuning recipe across all experiments. Specifically, we use AdamW with weight decay of 0.01 and global-norm gradient clipping of 1.0. The learning rate warms up linearly over the first 5% of training steps to its peak (η), then follows a cosine decay to $0.1 \times$ the peak over the remaining steps.

SFT setting. We experiment with five public base models:

Decoder-only language models. For instruction tuning, we tune Llama-3.2-1B [18] on the Tulu-3 supervised finetuning mixture [43]. For long-context reasoning, we train Qwen2.5-3B-Instruct [64] on the OpenThoughts-114k [19].

Encoder-only models. We finetune RoBERTa-large [55] on the ANLI benchmark [60] and adapt ViT-Huge/14 [15] to ImageNet-1K [11]. Following prior work [21], we fix the learning rate of the classification head at 10^{-3} and sweep only the LoRA learning rate.

Vision-language model. For multimodal instruction following, we finetune Qwen3-VL-2B-Instruct [1] on LLaVA-Instruct-Mix, containing image–instruction pairs.

RLVR setting. We adapt Llama-3.1-8B [18] to GSM8k [8] with GRPO [71]. The reward is based on answer correctness and format compliance.

Text-to-image diffusion model finetuning. We finetune Stable-Diffusion-v1.5 [69] on the Naruto-BLIP-Captions [6] dataset.

Evaluation protocol. We compare three LoRA configurations: Init[A] with $\alpha = 1$, Init[A] with $\alpha = r^{-1}$, and Init[B] with $\alpha = 1$. For each configuration, we sweep learning rate η (peak learning rate) on a \log_2 -scale grid with multiplicative steps of $2 \times$ and select the best value independently for (i) final training loss (EMA-smoothed) and (ii) a task-specific validation metric. For RLVR, we select learning rates by final training reward; for diffusion models, by validation FID [33]. More details are in Appendix B. We report training-loss-based sweeps in the main text and defer the other results to Appendix C, D, E.

Theory–experiment alignment. Our scaling rules characterize the leading-order dependence of the stable learning rate on width n and rank r in the joint limit $(n, r) \rightarrow \infty$. In practice, however, finetuning at finite width and rank introduces two deviations from the asymptotic prediction.

Finite-size effects. When (n, r) are finite, constant factors and lower-order terms can shift the optimal learning rate. These shifts are more pronounced for smaller ranks, where the large- r asymptotics are less accurate.

Discrete learning rate grid. We sweep learning rates on a \log_2 -spaced grid. The reported optimum is the best value among discrete points. When the loss landscape is flat near the true optimum, adjacent grid points perform similarly, and training noise may determine which one appears best.

Accordingly, we evaluate the scaling rules by qualitative

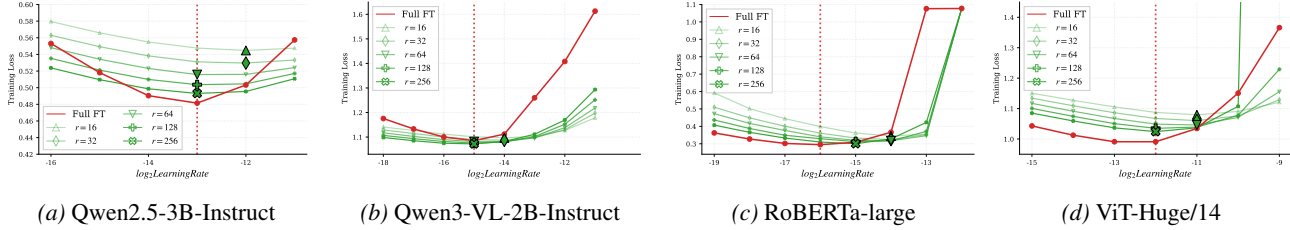


Figure 5. Learning rate sweeps for Init[B] with $\alpha = 1$ across four models. Curves show final training loss (EMA-smoothed) versus log-scale learning rate ($\log_2(\eta)$) for multiple ranks (green) and FFT (red). Large markers denote per-rank optima. The Y-axis is clipped for readability. The red vertical dashed line marks the optimal FFT learning rate.

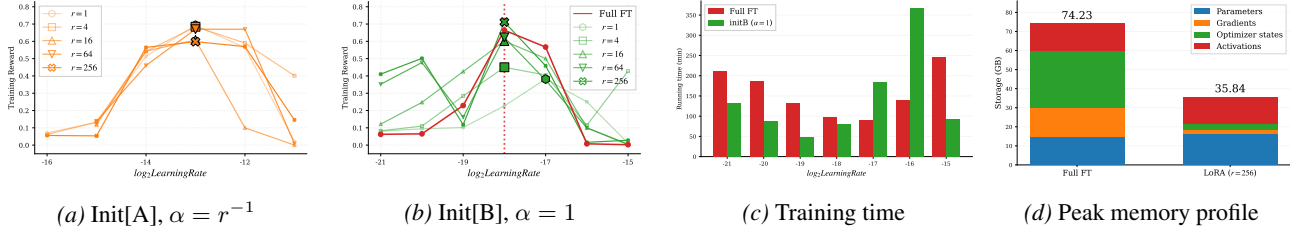


Figure 6. RLVR results on Llama-3.1-8B (GSM8k) with GRPO. (a)–(b) Learning rate sweeps plotting final training reward versus $\log_2(\eta)$. Large markers denote the best learning rate per rank; the red dashed line marks the FFT optimum. (c) Training time versus learning rate for FFT (red) and Init[B] with $\alpha=1$ and $r=256$ (green). (d) Peak GPU memory breakdown for FFT (left) and LoRA with $r=256$ (right).

trends rather than exact numerical agreement. For configurations predicted to be rank-invariant, we expect optimal learning rates to cluster within one grid step ($2\times$). For rank-dependent configurations, we expect the optimum to change monotonically with rank and to span multiple grid points.

5.2. SFT Results

Init[A] with $\alpha = 1$ (Figures 3, 2a) For a fixed base model (i.e., fixed width n), our theory in Table 1 predicts that the optimal learning rate scales as $\eta \propto r^{-1/2}$ with rank. This prediction is broadly supported by the experiments: as rank increases, the best-performing learning rate monotonically shifts toward smaller values. Since each figure plots $\log_2(\eta)$ on the X-axis, a $4\times$ increase in rank should shift the optimum leftward by one unit (i.e., a $2\times$ reduction in learning rate)—a pattern clearly visible across most models. We observe minor deviations on Qwen2.5-3B-Instruct, where both $r = 16$ and $r = 64$ attain their minimum loss at the same learning rate. We attribute this to the learning rate grid discretization: as shown in Figure 3a, the loss curves for $r = 4$ and $r = 16$ flatten near the optimum. Moreover, models finetuned with Init[A] and $\alpha = 1$ are sensitive to large learning rates: increasing the learning rate by $2\times$ beyond the optimum can substantially degrade training loss or cause divergence, particularly for Qwen2.5-3B-Instruct and RoBERTa-large.

While we report results for $\alpha = 1$ here, our theory holds for any rank-independent constant α . Since $\alpha = 2$ is a common default in practice, we verify in Appendix C.1 that the same

scaling behavior persists for $\alpha \in \{2, 4\}$.

Init[A] with $\alpha = r^{-1}$ (Figures 4, 2b) According to our theory, for a fixed base model, the optimal learning rate should be independent of LoRA rank under this setting. The experimental results support this prediction: for all models, the optimal learning rates across ranks fall within a narrow range (typically within $2\times$), consistent with rank-invariance. As with Init[A] and $\alpha = 1$, this small variation is attributable to the discrete learning rate grid. Compared to the $\alpha = 1$ setting, the optimal learning rates under $\alpha = r^{-1}$ are substantially larger. We also observe that smaller ranks (e.g., $r = 4$) usually favor slightly smaller learning rates than larger ranks—opposite to the trend observed with $\alpha = 1$. This likely reflects the finite-size effects: at smaller ranks, lower-order terms can exert a non-negligible influence on feature learning and suppress the optimal learning rate.

Init[B] with $\alpha = 1$ (Figures 5, 2c) In this case, the optimal learning rate should be independent of LoRA rank. The empirical results confirm this prediction: across all models, the best learning rates for different ranks cluster tightly. The small variation likely stems from learning rate grid resolution and finite-size effects. Although both Init[B] with $\alpha = 1$ and Init[A] with $\alpha = r^{-1}$ exhibit rank-invariant optimal learning rates, our theory shows they differ in width scaling: $\eta \propto n^{-1}$ for the former versus $\eta \propto n^{-1/2}$ for the latter. For large n , Init[B] thus requires substantially smaller learning rates, as our experiments confirm. We also observe that Init[B] with $\alpha = 1$ is more tolerant of larger learning

rates. This stability is consistent with the theoretical finding that intermediate features remain order-one under Init[B] , preventing internal activations from growing with width.

Crucially, our theory reveals that FFT shares the same learning rate scaling $\eta \propto n^{-1}$ with Init[B] with $\alpha = 1$, suggesting that their optimal learning rates may align and leading to learning rate transfer between the two. Experiments support this conjecture: for most models, the optimal learning rates for Init[B] ($\alpha = 1$) align closely with those for FFT. The exception is RoBERTa-large, where FFT favors a slightly smaller learning rate than Init[B] . We attribute this gap to the additional classification head: although its learning rate is fixed, jointly training it with LoRA adapters may still perturb the optimal learning rate. Nevertheless, our experiments show that learning rates tuned for Init[B] with $\alpha = 1$ transfers effectively to FFT in most model architectures, with minimal performance degradation.

5.3. RLVR Results

RLVR results are reported in Figure 6. The learning rate sweeps reveal patterns consistent with our findings under SFT. Under Init[A] with $\alpha = r^{-1}$ (Figure 6a), the optimal learning rate is approximately rank-invariant: curves for different ranks peak at nearly the same learning rate. Similarly, under Init[B] with $\alpha = 1$ (Figure 6b), the optimal learning rate is rank-invariant and aligns with the FFT optimum, suggesting that learning rates tuned with LoRA can transfer seamlessly to FFT. For results of Init[A] with $\alpha = 1$, please kindly refer to Appendix D.1.

Compared with SFT, RL finetuning is more sensitive to learning rate selection. In SFT, a learning rate that is too small simply slows convergence; in RLVR, however, overly large or small learning rates substantially degrade training reward. Importantly, this sensitivity also manifests in training time. As shown in Figure 6c, the optimal learning rate incurs the shortest training time, while suboptimal rates can increase wall-clock time by 2–4×. The μA scaling rules thus provide practical value beyond final performance: by identifying well-behaved learning rate regions in advance, practitioners can avoid time-consuming hyperparameter searches over suboptimal configurations. We provide a detailed investigation on this phenomenon in Appendix D.2.

Although LoRA and FFT have comparable per-step wall-clock times in our experiment, their memory footprints differ substantially. Figure 6d shows that FFT consumes over 2× the GPU memory of LoRA ($r=256$), with most overhead attributable to gradient buffers and optimizer states. This gap widens further at larger model sizes. Our theory thus enables a practical workflow that exploits this difference: one can sweep learning rates using Init[B] with $\alpha=1$ on mid-tier GPUs (e.g., A6000), which are more available and cost-effective, then transfer the optimal rate directly to

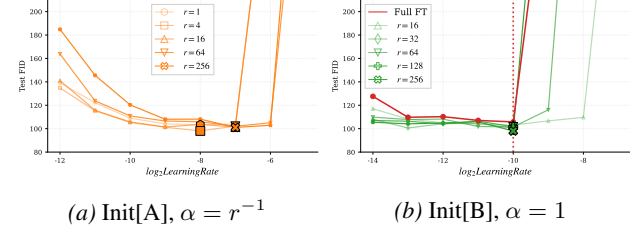


Figure 7. Results on Stable-Diffusion-1.5 (naruto-blip-captions). Subfigures plot validation FID score versus log-scale learning rate ($\log_2(\eta)$). Large markers denote the best learning rate for each rank; the red vertical dashed line marks the FFT optimum.

FFT on higher-capacity hardware with minimal re-tuning.

5.4. Text-to-Image Diffusion Finetuning Results

Figure 7 summarizes the results for finetuning a stable diffusion model. The learning rate sweeps show patterns consistent with our theory: under Init[A] with $\alpha = r^{-1}$, the optimal learning rate is rank-invariant, while under Init[B] with $\alpha = 1$, the optimal learning rate remains independent of rank and aligns with that of FFT. Notably, FFT is more sensitive to learning rate selection on diffusion models, exhibiting a sharp increase in validation FID at higher learning rates. This may be due to the UNet architecture’s blocks of varying width, which amplify sensitivity under FFT. Additional results for Init[A] with $\alpha = 1$ are in Appendix E.1.

6. Conclusion and Limitations

This work proposes μA (Maximal-Update Adaptation), a theoretical framework for LoRA finetuning that characterizes how the optimal learning rate scales with model width and adapter rank to achieve maximal feature updates. Using this framework, we identify a LoRA configuration that enables learning rate transfer between LoRA and FFT. Comprehensive experiments validate the μA scaling rules and demonstrate effective learning rate transfer in practice.

Our work has two main limitations. First, our theory is asymptotic and can be sensitive to noise for finite (n, r) . Second, our analysis establishes a necessary condition for learning rate transfer; future work is needed to identify and prove sufficient conditions for a more complete theory. Nevertheless, our experiments show strong agreement between theoretical predictions and empirical results.

Acknowledgment

This work used GPU servers at Delta AI (NCSA) through allocation #CIS250883 from the Advanced Cyberinfrastructure Coordination Ecosystem: Services & Support (ACCESS) program [4], which is supported by U.S. National Science Foundation grants #2138259, #2138286, #2138307, #2137603, and #2138296.

References

[1] Bai, S., Cai, Y., Chen, R., Chen, K., Chen, X., Cheng, Z., Deng, L., Ding, W., Gao, C., Ge, C., Ge, W., Guo, Z., Huang, Q., Huang, J., Huang, F., Hui, B., Jiang, S., Li, Z., Li, M., Li, M., Li, K., Lin, Z., Lin, J., Liu, X., Liu, J., Liu, C., Liu, Y., Liu, D., Liu, S., Lu, D., Luo, R., Lv, C., Men, R., Meng, L., Ren, X., Ren, X., Song, S., Sun, Y., Tang, J., Tu, J., Wan, J., Wang, P., Wang, P., Wang, Q., Wang, Y., Xie, T., Xu, Y., Xu, H., Xu, J., Yang, Z., Yang, M., Yang, J., Yang, A., Yu, B., Zhang, F., Zhang, H., Zhang, X., Zheng, B., Zhong, H., Zhou, J., Zhou, F., Zhou, J., Zhu, Y., and Zhu, K. Qwen3-vl technical report, 2025. URL <https://arxiv.org/abs/2511.21631>.

[2] Bernstein, J., Wang, Y., Azizzadenesheli, K., and Anandkumar, A. SIGNSGD: compressed optimisation for non-convex problems. In Dy, J. G. and Krause, A. (eds.), *Proceedings of the 35th International Conference on Machine Learning, ICML 2018, Stockholm, Sweden, July 10-15, 2018*, volume 80 of *Proceedings of Machine Learning Research*, pp. 559–568. PMLR, 2018. URL <http://proceedings.mlr.press/v80/bernstein18a.html>.

[3] Biderman, D., Portes, J., Ortiz, J. J. G., Paul, M., Greengard, P., Jennings, C., King, D., Havens, S., Chiley, V., Frankle, J., Blakeney, C., and Cunningham, J. P. LoRA learns less and forgets less. *Transactions on Machine Learning Research*, 2024. ISSN 2835-8856. URL <https://openreview.net/forum?id=aloEru2qCG>. Featured Certification.

[4] Boerner, T. J., Deems, S., Furlani, T. R., Knuth, S. L., and Towns, J. Access: Advancing innovation: Nsf’s advanced cyberinfrastructure coordination ecosystem: Services & support. In *Practice and Experience in Advanced Research Computing 2023: Computing for the Common Good*, PEARC ’23, pp. 173–176, New York, NY, USA, 2023. Association for Computing Machinery. ISBN 9781450399852. doi: 10.1145/3569951.3597559. URL <https://doi.org/10.1145/3569951.3597559>.

[5] Büyükköyüz, K. Olora: Orthonormal low-rank adaptation of large language models. *arXiv preprint arXiv:2406.01775*, 2024.

[6] Cervenka, E. Naruto blip captions. <https://huggingface.co/datasets/lambdalabs/naruto-blip-captions/>, 2022.

[7] Charakorn, R., Cetin, E., Tang, Y., and Lange, R. T. Text-to-lora: Instant transformer adaption. *arXiv preprint arXiv:2506.06105*, 2025.

[8] Cobbe, K., Kosaraju, V., Bavarian, M., Chen, M., Jun, H., Kaiser, L., Plappert, M., Tworek, J., Hilton, J., Nakano, R., Hesse, C., and Schulman, J. Training verifiers to solve math word problems. *arXiv preprint arXiv:2110.14168*, 2021.

[9] Collobert, R. and Weston, J. A unified architecture for natural language processing: Deep neural networks with multitask learning. In *Proceedings of the 25th international conference on Machine learning*, pp. 160–167, 2008.

[10] Dao, T. FlashAttention-2: Faster attention with better parallelism and work partitioning. In *International Conference on Learning Representations (ICLR)*, 2024.

[11] Deng, J., Dong, W., Socher, R., Li, L.-J., Li, K., and Fei-Fei, L. Imagenet: A large-scale hierarchical image database. In *2009 IEEE conference on computer vision and pattern recognition*, pp. 248–255. Ieee, 2009.

[12] Detlefsen, N. S., Borovac, J., Schock, J., Jha, A. H., Koker, T., Di Liello, L., Stancl, D., Quan, C., Grechkin, M., and Falcon, W. Torchmetrics-measuring reproducibility in pytorch. *Journal of Open Source Software*, 7(70):4101, 2022.

[13] Dettmers, T., Pagnoni, A., Holtzman, A., and Zettlemoyer, L. Qlora: Efficient finetuning of quantized llms. *Advances in neural information processing systems*, 36:10088–10115, 2023.

[14] Devlin, J., Chang, M.-W., Lee, K., and Toutanova, K. Bert: Pre-training of deep bidirectional transformers for language understanding. In *Proceedings of the 2019 conference of the North American chapter of the association for computational linguistics: human language technologies, volume 1 (long and short papers)*, pp. 4171–4186, 2019.

[15] Dosovitskiy, A., Beyer, L., Kolesnikov, A., Weissenborn, D., Zhai, X., Unterthiner, T., Dehghani, M., Minderer, M., Heigold, G., Gelly, S., Uszkoreit, J., and Houlsby, N. An image is worth 16x16 words: Transformers for image recognition at scale. In *International Conference on Learning Representations*, 2021. URL <https://openreview.net/forum?id=YicbFdNTTy>.

[16] Gabrielsson, R. B., Zhu, J., Bhardwaj, O., Choshen, L., Greenewald, K., Yurochkin, M., and Solomon, J. Compress then serve: Serving thousands of lora adapters with little overhead. In *Forty-second International Conference on Machine Learning*, 2024.

[17] Glorot, X. and Bengio, Y. Understanding the difficulty of training deep feedforward neural networks. In *Proceedings of the thirteenth international conference on artificial intelligence and statistics*, pp. 249–256. JMLR Workshop and Conference Proceedings, 2010.

[18] Grattafiori, A., Dubey, A., Jauhri, A., Pandey, A., Kadian, A., Al-Dahle, A., Letman, A., Mathur, A., Schellen, A., Vaughan, A., et al. The llama 3 herd of models. *arXiv preprint arXiv:2407.21783*, 2024.

[19] Guha, E., Marten, R., Keh, S., Raoof, N., Smyrnis, G., Bansal, H., Nezhurina, M., Mercat, J., Vu, T., Sprague, Z., et al. Openthoughts: Data recipes for reasoning models. *arXiv preprint arXiv:2506.04178*, 2025.

[20] Guo, D., Rush, A. M., and Kim, Y. Parameter-efficient transfer learning with diff pruning. In *Proceedings of the 59th Annual Meeting of the Association for Computational Linguistics and the 11th International Joint Conference on Natural Language Processing (Volume 1: Long Papers)*, pp. 4884–4896, 2021.

[21] Guo, Y., Sun, S., Ma, S., Zheng, K., Bao, X., Ma, S., Zou, W., and Zheng, Y. Crossmae: Cross-modality masked autoencoders for region-aware audio-visual pre-training. In *Proceedings of the IEEE/CVF Conference on Computer Vision and Pattern Recognition*, pp. 26721–26731, 2024.

[22] Han, Z., Gao, C., Liu, J., Zhang, J., and Zhang, S. Q. Parameter-efficient fine-tuning for large models: A comprehensive survey. *arXiv preprint arXiv:2403.14608*, 2024.

[23] Hayou, S. and Liu, L. Optimal embedding learning rate in llms: The effect of vocabulary size. *arXiv preprint arXiv:2506.15025*, 2025.

[24] Hayou, S. and Yang, G. Width and depth limits commute in residual networks. In *International Conference on Machine Learning*, pp. 12700–12723. PMLR, 2023.

[25] Hayou, S., Doucet, A., and Rousseau, J. On the impact of the activation function on deep neural networks training. In *International conference on machine learning*, pp. 2672–2680. PMLR, 2019.

[26] Hayou, S., Clerico, E., He, B., Deligiannidis, G., Doucet, A., and Rousseau, J. Stable resnet. In *International Conference on Artificial Intelligence and Statistics*, pp. 1324–1332. PMLR, 2021.

[27] Hayou, S., Ghosh, N., and Yu, B. The impact of initialization on lora finetuning dynamics. *Advances in Neural Information Processing Systems*, 37:117015–117040, 2024.

[28] Hayou, S., Ghosh, N., and Yu, B. Lora+: Efficient low rank adaptation of large models. *arXiv preprint arXiv:2402.12354*, 2024.

[29] Hayou, S., Ghosh, N., and Yu, B. Plop: Precise lora placement for efficient finetuning of large models. *arXiv preprint arXiv:2506.20629*, 2025.

[30] He, B., Martens, J., Zhang, G., Botev, A., Brock, A., Smith, S. L., and Teh, Y. W. Deep transformers without shortcuts: Modifying self-attention for faithful signal propagation. In *The Eleventh International Conference on Learning Representations*, 2023. URL <https://openreview.net/forum?id=NPrsUQgMjKK>.

[31] He, J., Zhou, C., Ma, X., Berg-Kirkpatrick, T., and Neubig, G. Towards a unified view of parameter-efficient transfer learning. In *International Conference on Learning Representations*, 2022. URL <https://openreview.net/forum?id=0RDcd5Axok>.

[32] He, K., Zhang, X., Ren, S., and Sun, J. Delving deep into rectifiers: Surpassing human-level performance on imagenet classification. In *Proceedings of the IEEE international conference on computer vision*, pp. 1026–1034, 2015.

[33] Heusel, M., Ramsauer, H., Unterthiner, T., Nessler, B., and Hochreiter, S. Gans trained by a two time-scale update rule converge to a local nash equilibrium. *Advances in neural information processing systems*, 30, 2017.

[34] Ho, J., Jain, A., and Abbeel, P. Denoising diffusion probabilistic models. *Advances in neural information processing systems*, 33:6840–6851, 2020.

[35] Houlsby, N., Giurgiu, A., Jastrzebski, S., Morrone, B., De Laroussilhe, Q., Gesmundo, A., Attariyan, M., and Gelly, S. Parameter-efficient transfer learning for nlp. In *International conference on machine learning*, pp. 2790–2799. PMLR, 2019.

[36] Hu, E. J., yelong shen, Wallis, P., Allen-Zhu, Z., Li, Y., Wang, S., Wang, L., and Chen, W. LoRA: Low-rank adaptation of large language models. In *International Conference on Learning Representations*, 2022. URL <https://openreview.net/forum?id=nZeVKeeFYf9>.

[37] Ji, W., Yuan, W., Getzen, E., Cho, K., Jordan, M. I., Mei, S., Weston, J. E., Su, W. J., Xu, J., and Zhang, L. An overview of large language models for statisticians. *arXiv preprint arXiv:2502.17814*, 2025.

[38] Kalajdzievski, D. A rank stabilization scaling factor for fine-tuning with lora. *arXiv preprint arXiv:2312.03732*, 2023.

[39] Ke, W., Wang, J., Wang, P., Liu, J., Nie, D., Li, G., and Li, Y. Unveiling lora intrinsic ranks via salience analysis. *Advances in Neural Information Processing Systems*, 37:131575–131595, 2024.

[40] Kingma, D. P. and Ba, J. Adam: A method for stochastic optimization. In Bengio, Y. and LeCun, Y. (eds.), *3rd International Conference on Learning Representations, ICLR 2015, San Diego, CA, USA, May 7-9, 2015, Conference Track Proceedings*, 2015. URL <http://arxiv.org/abs/1412.6980>.

[41] Kingma, D. P. and Welling, M. Auto-encoding variational bayes. In *2nd International Conference on Learning Representations, ICLR 2014*, 2014.

[42] Kopiczko, D. J., Blankevoort, T., and Asano, Y. M. VeRA: Vector-based random matrix adaptation. In *The Twelfth International Conference on Learning Representations*, 2024. URL <https://openreview.net/forum?id=NjNfLdxr3A>.

[43] Lambert, N., Morrison, J., Pyatkin, V., Huang, S., Iivison, H., Brahman, F., Miranda, L. J. V., Liu, A., Dziri, N., Lyu, S., et al. Tulu 3: Pushing frontiers in open language model post-training. *arXiv preprint arXiv:2411.15124*, 2024.

[44] Lester, B., Al-Rfou, R., and Constant, N. The power of scale for parameter-efficient prompt tuning. In *Proceedings of the 2021 Conference on Empirical Methods in Natural Language Processing*. Association for Computational Linguistics, 2021.

[45] Lhoest, Q., Villanova del Moral, A., Jernite, Y., Thakur, A., von Platen, P., Patil, S., Chaumond, J., Drame, M., Plu, J., Tunstall, L., Davison, J., Šaško, M., Chhabiani, G., Malik, B., Brandeis, S., Le Scao, T., Sanh, V., Xu, C., Patry, N., McMillan-Major, A., Schmid, P., Gugger, S., Delangue, C., Matussière, T., Debut, L., Bekman, S., Cistac, P., Goehringer, T., Mustar, V., Lagunas, F., Rush, A., and Wolf, T. Datasets: A community library for natural language processing. In *Proceedings of the 2021 Conference on Empirical Methods in Natural Language Processing: System Demonstrations*, pp. 175–184, Online and Punta Cana, Dominican Republic, November 2021. Association for Computational Linguistics. URL <https://aclanthology.org/2021.emnlp-demo.21>.

[46] Li, S., Luo, X., Tang, X., Wang, H., Chen, H., weihongluo, Li, Y., xiuqiang He, and Li, R. Beyond zero initialization: Investigating the impact of non-zero initialization on loRA fine-tuning dynamics. In *Forty-second International Conference on Machine Learning*, 2025. URL <https://openreview.net/forum?id=8V6METSn1R>.

[47] Li, X. L. and Liang, P. Prefix-tuning: Optimizing continuous prompts for generation. In *Proceedings of the 59th Annual Meeting of the Association for Computational Linguistics and the 11th International Joint Conference on Natural Language Processing (Volume 1: Long Papers)*. Association for Computational Linguistics, 2021.

[48] Li, Y., Han, S., and Ji, S. Vb-lora: Extreme parameter efficient fine-tuning with vector banks. *Advances in Neural Information Processing Systems*, 37:16724–16751, 2024.

[49] Li, Y., Yu, Y., Liang, C., Karampatziakis, N., He, P., Chen, W., and Zhao, T. Loftq: LoRA-fine-tuning-aware quantization for large language models. In *The Twelfth International Conference on Learning Representations*, 2024. URL <https://openreview.net/forum?id=LzPWWPAy4>.

[50] Liao, B., Meng, Y., and Monz, C. Parameter-efficient fine-tuning without introducing new latency. In *Proceedings of the 61st Annual Meeting of the Association for Computational Linguistics (Volume 1: Long Papers)*, pp. 4242–4260, 2023.

[51] Lin, Z., Madotto, A., and Fung, P. Exploring versatile generative language model via parameter-efficient transfer learning. In *Findings of the Association for Computational Linguistics: EMNLP 2020*, pp. 441–459, 2020.

[52] Liu, A., Feng, B., Xue, B., Wang, B., Wu, B., Lu, C., Zhao, C., Deng, C., Zhang, C., Ruan, C., et al. Deepseek-v3 technical report. *arXiv preprint arXiv:2412.19437*, 2024.

[53] Liu, S.-Y., Wang, C.-Y., Yin, H., Molchanov, P., Wang, Y.-C. F., Cheng, K.-T., and Chen, M.-H. Dora: Weight-decomposed low-rank adaptation. In *Forty-first International Conference on Machine Learning*, 2024.

[54] Liu, X., Zheng, Y., Du, Z., Ding, M., Qian, Y., Yang, Z., and Tang, J. Gpt understands, too, 2023. URL <https://arxiv.org/abs/2103.10385>.

[55] Liu, Y., Ott, M., Goyal, N., Du, J., Joshi, M., Chen, D., Levy, O., Lewis, M., Zettlemoyer, L., and Stoyanov, V. Roberta: A robustly optimized bert pretraining approach. *arXiv preprint arXiv:1907.11692*, 2019.

[56] Loshchilov, I. and Hutter, F. Decoupled weight decay regularization. In *7th International Conference on Learning Representations, ICLR 2019, New Orleans, LA, USA, May 6-9, 2019*. OpenReview.net, 2019. URL <https://openreview.net/forum?id=Bkg6RiCqY7>.

[57] Mangrulkar, S., Gugger, S., Debut, L., Belkada, Y., Paul, S., Bossan, B., and Tietz, M. PEFT: State-of-the-art parameter-efficient fine-tuning methods. <https://github.com/huggingface/peft>, 2022.

[58] Meng, F., Wang, Z., and Zhang, M. Pissa: Principal singular values and singular vectors adaptation of large language models. *Advances in Neural Information Processing Systems*, 37:121038–121072, 2024.

[59] Milsom, E., Anson, B., and Aitchison, L. Function-space learning rates, 2025. URL <https://arxiv.org/abs/2502.17405>.

[60] Nie, Y., Williams, A., Dinan, E., Bansal, M., Weston, J., and Kiela, D. Adversarial nli: A new benchmark for natural language understanding. In *Proceedings of the 58th Annual Meeting of the Association for Computational Linguistics*. Association for Computational Linguistics, 2020.

[61] Noci, L., Li, C., Li, M., He, B., Hofmann, T., Mad-dison, C. J., and Roy, D. The shaped transformer: Attention models in the infinite depth-and-width limit. *Advances in Neural Information Processing Systems*, 36:54250–54281, 2023.

[62] Paischer, F., Hauzenberger, L., Schmied, T., Alkin, B., Deisenroth, M. P., and Hochreiter, S. One initialization to rule them all: Fine-tuning via explained variance adaptation. *arXiv preprint arXiv:2410.07170*, 2024.

[63] Paszke, A., Gross, S., Massa, F., Lerer, A., Bradbury, J., Chanan, G., Killeen, T., Lin, Z., Gimelshein, N., Antiga, L., et al. Pytorch: An imperative style, high-performance deep learning library. *Advances in neural information processing systems*, 32, 2019.

[64] Qwen, :, Yang, A., Yang, B., Zhang, B., Hui, B., Zheng, B., Yu, B., Li, C., Liu, D., Huang, F., Wei, H., Lin, H., Yang, J., Tu, J., Zhang, J., Yang, J., Yang, J., Zhou, J., Lin, J., Dang, K., Lu, K., Bao, K., Yang, K., Yu, L., Li, M., Xue, M., Zhang, P., Zhu, Q., Men, R., Lin, R., Li, T., Tang, T., Xia, T., Ren, X., Ren, X., Fan, Y., Su, Y., Zhang, Y., Wan, Y., Liu, Y., Cui, Z., Zhang, Z., and Qiu, Z. Qwen2.5 technical report, 2025. URL <https://arxiv.org/abs/2412.15115>.

[65] Radford, A., Narasimhan, K., Salimans, T., Sutskever, I., et al. Improving language understanding by generative pre-training. 2018. OpenAI Technical Report.

[66] Radford, A., Kim, J. W., Hallacy, C., Ramesh, A., Goh, G., Agarwal, S., Sastry, G., Askell, A., Mishkin, P., Clark, J., et al. Learning transferable visual models from natural language supervision. In *International conference on machine learning*, pp. 8748–8763. PMLR, 2021.

[67] Raffel, C., Shazeer, N., Roberts, A., Lee, K., Narang, S., Matena, M., Zhou, Y., Li, W., and Liu, P. J. Exploring the limits of transfer learning with a unified text-to-text transformer. *Journal of machine learning research*, 21(140):1–67, 2020.

[68] Rebuffi, S.-A., Bilen, H., and Vedaldi, A. Learning multiple visual domains with residual adapters. *Advances in neural information processing systems*, 30, 2017.

[69] Rombach, R., Blattmann, A., Lorenz, D., Esser, P., and Ommer, B. High-resolution image synthesis with latent diffusion models. In *Proceedings of the IEEE/CVF Conference on Computer Vision and Pattern Recognition (CVPR)*, pp. 10684–10695, June 2022.

[70] Schulman, J. Lora without regret. *Thinking Machines Lab: Connectionism*, 2025. doi: 10.64434/tm1.20250929. <https://thinkingmachines.ai/blog/lora/>.

[71] Shao, Z., Wang, P., Zhu, Q., Xu, R., Song, J., Bi, X., Zhang, H., Zhang, M., Li, Y., Wu, Y., et al. Deepseekmath: Pushing the limits of mathematical reasoning in open language models. *arXiv preprint arXiv:2402.03300*, 2024.

[72] Shuttleworth, R., Andreas, J., Torralba, A., and Sharma, P. Lora vs full fine-tuning: An illusion of equivalence. *arXiv preprint arXiv:2410.21228*, 2024.

[73] Szegedy, C., Vanhoucke, V., Ioffe, S., Shlens, J., and Wojna, Z. Rethinking the inception architecture for computer vision. In *Proceedings of the IEEE conference on computer vision and pattern recognition*, pp. 2818–2826, 2016.

[74] Team, G., Kamath, A., Ferret, J., Pathak, S., Vieillard, N., Merhej, R., Perrin, S., Matejovicova, T., Ramé, A., Rivière, M., et al. Gemma 3 technical report. *arXiv preprint arXiv:2503.19786*, 2025.

[75] TorchVision. Torchvision: Pytorch’s computer vision library. <https://github.com/pytorch/vision>, 2016.

[76] Tschannen, M., Gritsenko, A., Wang, X., Naeem, M. F., Alabdulmohsin, I., Parthasarathy, N., Evans, T., Beyer, L., Xia, Y., Mustafa, B., et al. Siglip 2: Multilingual vision-language encoders with improved semantic understanding, localization, and dense features. *arXiv preprint arXiv:2502.14786*, 2025.

[77] Valipour, M., Rezagholizadeh, M., Kobyzhev, I., and Ghodsi, A. Dylora: Parameter-efficient tuning of pre-trained models using dynamic search-free low-rank adaptation. In *Proceedings of the 17th Conference of the European Chapter of the Association for Computational Linguistics*, pp. 3274–3287, 2023.

[78] von Platen, P., Patil, S., Lozhkov, A., Cuenca, P., Lambert, N., Rasul, K., Davaadorj, M., Nair, D., Paul, S., Berman, W., Xu, Y., Liu, S., and Wolf, T. Diffusers: State-of-the-art diffusion models. <https://github.com/huggingface/diffusers>, 2022.

[79] von Werra, L., Belkada, Y., Tunstall, L., Beeching, E., Thrush, T., Lambert, N., Huang, S., Rasul, K., and Gallouédec, Q. TRL: Transformers Reinforcement Learning, 2020. URL <https://github.com/huggingface/trl>.

[80] Wang, S., Yu, L., and Li, J. Lora-ga: Low-rank adaptation with gradient approximation. *Advances in Neural Information Processing Systems*, 37:54905–54931, 2024.

[81] Wang, Z., Liang, J., He, R., Wang, Z., and Tan, T. LoRA-pro: Are low-rank adapters properly optimized? In *The Thirteenth International Conference on Learning Representations*, 2025. URL <https://openreview.net/forum?id=gTwRMU31J5>.

[82] Wolf, T., Debut, L., Sanh, V., Chaumond, J., Delangue, C., Moi, A., Cistac, P., Rault, T., Louf, R., Funtowicz, M., Davison, J., Shleifer, S., von Platen, P., Ma, C., Jernite, Y., Plu, J., Xu, C., Scao, T. L., Gugger, S., Drame, M., Lhoest, Q., and Rush, A. M. Transformers: State-of-the-art natural language processing. In *Proceedings of the 2020 Conference on Empirical Methods in Natural Language Processing: System Demonstrations*, pp. 38–45, Online, October 2020. Association for Computational Linguistics. URL <https://www.aclweb.org/anthology/2020.emnlp-demos.6>.

[83] Yang, A., Li, A., Yang, B., Zhang, B., Hui, B., Zheng, B., Yu, B., Gao, C., Huang, C., Lv, C., et al. Qwen3 technical report. *arXiv preprint arXiv:2505.09388*, 2025.

[84] Yang, G. and Hu, E. J. Feature learning in infinite-width neural networks. *arXiv preprint arXiv:2011.14522*, 2020.

[85] Yang, G. and Hu, E. J. Tensor programs iv: Feature learning in infinite-width neural networks. In *International Conference on Machine Learning*, pp. 11727–11737. PMLR, 2021.

[86] Yang, G., Hu, E., Babuschkin, I., Sidor, S., Liu, X., Farhi, D., Ryder, N., Pachocki, J., Chen, W., and Gao, J. Tuning large neural networks via zero-shot hyperparameter transfer. *Advances in Neural Information Processing Systems*, 34:17084–17097, 2021.

[87] Yang, G., Yu, D., Zhu, C., and Hayou, S. Tensor programs VI: Feature learning in infinite depth neural networks. In *The Twelfth International Conference on Learning Representations*, 2024. URL <https://openreview.net/forum?id=17pVDnpww1>.

[88] Yang, Y., Li, X., Zhou, Z., Song, S., Wu, J., Nie, L., and Ghanem, B. Corda: Context-oriented decomposition adaptation of large language models for task-aware parameter-efficient fine-tuning. *Advances in Neural Information Processing Systems*, 37:71768–71791, 2024.

[89] Yen, J.-N., Si, S., Meng, Z., Yu, F., Duvvuri, S. S., Dhillon, I. S., Hsieh, C.-J., and Kumar, S. LoRA done RITE: Robust invariant transformation equilibration for LoRA optimization. In *The Thirteenth International Conference on Learning Representations*, 2025. URL <https://openreview.net/forum?id=VpWk1v2P8>.

[90] Yu, Q., Zhang, Z., Zhu, R., Yuan, Y., Zuo, X., Yue, Y., Dai, W., Fan, T., Liu, G., Liu, L., et al. Dapo: An open-source llm reinforcement learning system at scale. *arXiv preprint arXiv:2503.14476*, 2025.

[91] Zeng, Y. and Lee, K. The expressive power of low-rank adaptation. In *The Twelfth International Conference on Learning Representations*, 2024. URL <https://openreview.net/forum?id=likXVjmh3E>.

[92] Zhang, Q., Chen, M., Bukharin, A., Karampatziakis, N., He, P., Cheng, Y., Chen, W., and Zhao, T. Adalora: Adaptive budget allocation for parameter-efficient fine-tuning. *arXiv preprint arXiv:2303.10512*, 2023.

[93] Zhang, Z., Li, H., Zhang, Y., Gong, G., Wang, J., pengzhang liu, Jiang, Q., and Hu, J. The primacy of magnitude in low-rank adaptation. In *The Thirty-ninth Annual Conference on Neural Information Processing Systems*, 2025. URL <https://openreview.net/forum?id=s4LnWgjacg>.

A. Theoretical Proofs and Derivations for μ A

Purpose and scope. This appendix provides the detailed derivations supporting the theories in the main text. We analyze the dynamics of LoRA finetuning in the limit where both the network width n and the LoRA rank r grow to infinity. Our first goal is to ensure that the output features remain bounded throughout finetuning—that is, they do not explode as n and r increase. Achieving this requires scaling the learning rate appropriately with n and r . Our second goal is to ensure that the feature updates remain non-vanishing, so that learning proceeds efficiently and does not stall as the network grows.

A.1. Preliminaries and Notation Recap

We begin by briefly restating the notation used in the main text to make the appendix self-contained.

A.1.1. ASYMPTOTIC NOTATION AND SCALING CONVENTIONS

Definition A.1 (Asymptotic notation). For sequences $c_{n,r} \in \mathbb{R}$ and $d_{n,r} \in \mathbb{R}_+$, we write $c_{n,r} = \mathcal{O}(d_{n,r})$ (resp. $c_{n,r} = \Omega(d_{n,r})$) if there exist constants $\kappa > 0$ and $N \in \mathbb{N}$ such that for all $n, r > N$ with $r \leq n$, we have $|c_{n,r}| < \kappa d_{n,r}$ (resp. $|c_{n,r}| > \kappa d_{n,r}$). We write $c_{n,r} = \Theta(d_{n,r})$ if both bounds hold. This notation extends element-wise to vectors: for $c_{n,r} = (c_{n,r}^i)_{i=1}^k \in \mathbb{R}^k$ and $d_{n,r} = (d_{n,r}^i)_{i=1}^k \in \mathbb{R}_+^k$, we write $c_{n,r} = \mathcal{O}(d_{n,r})$ when $c_{n,r}^i = \mathcal{O}(d_{n,r}^i)$ for all $i \in [k]$, and similarly for Ω and Θ . For random variables, the notation is understood in the second-moment sense: $c_{n,r} = \mathcal{O}(d_{n,r})$ means $(\mathbb{E}|c_{n,r}|^2)^{1/2} = \mathcal{O}(d_{n,r})$.

Fixed training regime. All results are proved for a fixed training horizon T that does not scale with (n, r) .

A.1.2. LORA LAYER, FEATURES, AND THE PER-STEP DECOMPOSITION

Definition A.2 (Low-Rank Adaptation (LoRA)). Let $W^* \in \mathbb{R}^{n \times n}$ be a pretrained weight matrix that remains fixed during finetuning. LoRA parameterizes the finetuned weights as

$$W = W^* + \alpha B A,$$

where $B \in \mathbb{R}^{n \times r}$ and $A \in \mathbb{R}^{r \times n}$ are trainable factors with rank $r \ll n$ and $\alpha \in \mathbb{R}$ is a scalar multiplier.

For a given layer augmented with a LoRA adaptor, we use \underline{Z} and \bar{Z} to denote the input and output of the layer, respectively. Specifically, we can write the layer operation as $\bar{Z} = W^* \underline{Z} + \alpha B A \underline{Z}$. In addition, we use $d\bar{Z}$ to denote the backpropagated gradient of the loss with respect to \bar{Z} , i.e., $d\bar{Z} = \partial \mathcal{L} / \partial \bar{Z}$. Next, we define the following intermediate and output features.

Definition A.3 (LoRA features). For a layer input \underline{Z} , define the intermediate and output LoRA features

$$Z_A := A \underline{Z} \in \mathbb{R}^r, \quad Z_B := \alpha B Z_A = \alpha B A \underline{Z} \in \mathbb{R}^n.$$

For $t \leq T$, we use superscripts to denote LoRA features at step t , i.e. Z_A^t , Z_B^t and subscripts to denote weights at step t , i.e. A_t , B_t . To isolate the contribution of individual LoRA layers to feature learning, we assume that only a single LoRA layer is trainable while all other layers remain fixed. Under this assumption, the layer input \underline{Z} remains unchanged across finetuning steps. After step t , the update to Z_B decomposes as:

$$\Delta Z_B^t = \underbrace{\alpha B_{t-1} \Delta Z_A^t}_{\delta_t^1} + \underbrace{\alpha \Delta B_t Z_A^{t-1}}_{\delta_t^2} + \underbrace{\alpha \Delta B_t \Delta Z_A^t}_{\delta_t^3} \quad (2)$$

Next, we give the formal definition of the initialization schemes considered in this work.

Definition A.4 (Initialization schemes for LoRA). To initialize the LoRA update as a no-op, we consider:

- **Init[A]:** A_0 has i.i.d. entries $\mathcal{N}(0, 1/n)$ and $B_0 = 0$.
- **Init[B]:** B_0 has i.i.d. entries $\mathcal{N}(0, 1/r)$ and $A_0 = 0$.

A.1.3. STABILITY AND NON-VANISHING LEARNING CRITERIA

Definition A.5 (Feature stability). Fix a finite number of finetuning steps T independent of (n, r) . We say LoRA finetuning is *stable* if for all steps $t \leq T$, we have $Z_B^t = \mathcal{O}(1)$ in the joint limit $n, r \rightarrow \infty$ with $r \leq n$.

Lemma A.6 (Telescoping bound). *Fix $t \leq T$. If $Z_B^0 = \mathcal{O}(1)$ and $\Delta Z_B^s = \mathcal{O}(1)$ for all $s \leq t$, then $Z_B^t = \mathcal{O}(1)$.*

Proof. By telescoping, $Z_B^t = Z_B^0 + \sum_{s=1}^t \Delta Z_B^s$. For a fixed t , this is a sum of $Z_B^0 = \mathcal{O}(1)$ and finitely many $\mathcal{O}(1)$ terms, hence $\mathcal{O}(1)$. \square

Since the LoRA adapter is typically initialized as a no-op (i.e., $Z_B^0 = 0$), Lemma A.6 implies that bounding the feature updates $\Delta Z_B^s = \mathcal{O}(1)$ is sufficient to ensure bounded features $Z_B^t = \mathcal{O}(1)$. Thus, verifying stability (Definition A.5) reduces to verifying that the updates remain bounded. However, to avoid trivial updates, we also require ΔZ_B^s to be of non-vanishing magnitude. This leads to the following definition:

Definition A.7 (Stable feature learning with LoRA). We say LoRA induces *stable feature learning* if the dynamics are stable (Definition A.5), and $\Delta Z_B^t = \Theta(1)$ for all $t \leq T$.

As shown in Equation (2), the feature update ΔZ_B^t decomposes into three terms $(\delta_t^i)_{i \in \{1, 2, 3\}}$. A *sufficient* condition for feature stability is the term-wise bound $\delta_t^i = \mathcal{O}(1)$ for all $i \in \{1, 2, 3\}$, which avoids relying on cancellations between terms. Stable feature learning additionally requires $\Delta Z_B^t = \Theta(1)$; under the term-wise control above, this in particular implies that at least one term must satisfy $\delta_t^i = \Omega(1)$. Efficiency imposes a stronger requirement: each term must be exactly $\Theta(1)$, ensuring that both weight matrices A and B contribute meaningfully to the update. We formalize this as follows:

Definition A.8 (Efficient Feature Learning with LoRA). We say that LoRA finetuning is efficient if it induces stable feature learning (Definition A.7), and for all finetuning steps $t \leq T$, we have:

$$\delta_t^i = \Theta(1), \quad i \in \{1, 2, 3\}.$$

A.2. Technical Setup

A.2.1. ASSUMPTIONS ON TRAINING DYNAMICS

Assumption A.9 (Bounded forward/backward signals). For any fixed step $t \leq T$, the layer input and the backpropagated output gradient satisfy

$$\underline{Z} = \Theta(1), \quad d\bar{Z} := \frac{\partial \mathcal{L}}{\partial \bar{Z}} = \Theta(1).$$

This ensures that features and gradients neither explode nor vanish at any step as $(n, r) \rightarrow \infty$.

Assumption A.10 (Optimizer abstraction). We use a simplified variant of Adam [40] without momentum, reducing it to SignSGD [2], which gives element-wise sign updates:

$$g_A^t := \text{sign}\left(\frac{\partial \mathcal{L}_t}{\partial A_{t-1}}\right), \quad g_B^t := \text{sign}\left(\frac{\partial \mathcal{L}_t}{\partial B_{t-1}}\right),$$

and parameter updates

$$A_t = A_{t-1} - \eta g_A^t, \quad B_t = B_{t-1} - \eta g_B^t,$$

where $\text{sign}(\cdot)$ is applied element-wise (with $\text{sign}(0) = 0$) and η denotes the learning rate.

At a specific training step t , we would have:

$$\frac{\partial \mathcal{L}_t}{\partial A_{t-1}} = \alpha(B_{t-1}^\top d\bar{Z}^{t-1}) \otimes \underline{Z} \quad (3)$$

$$\frac{\partial \mathcal{L}_t}{\partial B_{t-1}} = \alpha d\bar{Z}^{t-1} \otimes Z_A^{t-1} \quad (4)$$

where \otimes denotes outer product.

Following [27], we also consider the single-sample loss setting. This simplifies the theoretical analysis and leads to closed-form expressions.

A.2.2. AUXILIARY LEMMAS

This section contains auxiliary lemmas that are used as intermediate steps in the following analysis.

Lemma A.11 (Recursive Formulas). *For t fixed, the asymptotic dynamics of Z_A^t and B_t follow the recursive formula:*

$$Z_A^t = \max(\Theta(Z_A^{t-1}), \Theta(\eta n)) \quad (5)$$

$$B_t = \max(\Theta(B_{t-1}), \Theta(\eta)) \quad (6)$$

Proof. Let $S^t = \alpha B_{t-1}^\top d\bar{Z}^{t-1}$. We, from Eq. 3, have:

$$\begin{aligned} g_A^t &= \text{sign}(S^t \otimes \underline{Z}) \\ &= \text{sign}(S^t) \otimes \text{sign}(\underline{Z}) \end{aligned}$$

where in the second equation we use the fact that both S^t and \underline{Z} are both vectors. Hence, we obtain:

$$\begin{aligned} g_A^t \underline{Z} &= (\text{sign}(S^t) \otimes \text{sign}(\underline{Z})) \underline{Z} \\ &= (\text{sign}(\underline{Z})^\top \underline{Z}) \text{sign}(S^t) \\ &= \Theta(n) \end{aligned}$$

where we used the fact that $\text{sign}(\underline{Z})^\top \underline{Z} = \|\underline{Z}\|_1 = \Theta(n)$ and $\text{sign}(\cdot) = \Theta(1)$ due to the sign operator. Combining, we obtain Eq. 5:

$$\begin{aligned} Z_A^t &= \Theta((A_{t-1} - \eta g_A^t) \underline{Z}) \\ &= \Theta(Z_A^{t-1} - \eta g_A^t \underline{Z}) \\ &= \max(\Theta(Z_A^{t-1}), \Theta(\eta n)) \end{aligned}$$

Similarly, we have the following result for B_t :

$$\begin{aligned} B_t &= \Theta(B_{t-1} - \eta g_B^t) \\ &= \Theta(B_{t-1} - \eta \text{sign}(\frac{\partial \mathcal{L}_t}{\partial B_{t-1}})) \\ &= \max(\Theta(B_{t-1}), \Theta(\eta)) \end{aligned}$$

□

We take the next lemma from [23], and we restate it and show its proof to make this proof self-contained.

Lemma A.12 (Stein's lemma for a sign–Gaussian product). *Let (Z, G) be a bi-variate centered Gaussian vector with $\text{Var}(Z) = \text{Var}(G) = 1$ and correlation $\rho = \mathbb{E}[ZG]$. Then*

$$\mathbb{E}[\text{sign}(Z)G] = \rho \sqrt{\frac{2}{\pi}}$$

Proof. For a pair of standard Gaussians with correlation ρ , we have:

$$G = \rho Z + \sqrt{1 - \rho^2} G'$$

where $G' \sim \mathcal{N}(0, 1)$ is another standard Gaussian independent of Z . Putting it into the expectation:

$$\begin{aligned} \mathbb{E}[\text{sign}(Z)G] &= \mathbb{E}[\text{sign}(Z)(\rho Z + \sqrt{1 - \rho^2} G')] \\ &= \mathbb{E}[\rho \text{sign}(Z)Z] + \sqrt{1 - \rho^2} \cdot \mathbb{E}[\text{sign}(Z)G'] \\ &= \rho \mathbb{E}[\text{sign}(Z)Z] \\ &= \rho \mathbb{E}|Z| \end{aligned}$$

Since $Z \sim \mathcal{N}(0, 1)$, $\mathbb{E}|Z| = \sqrt{\frac{2}{\pi}}$. Plugging this in, we obtain:

$$\mathbb{E}[\text{sign}(Z)G] = \rho \sqrt{\frac{2}{\pi}}$$

□

Corollary A.13 (General sign–Gaussian product). *Let (Z, G) be a bi-variate centered Gaussian vector with $\text{Var}(Z) = \sigma_Z^2$ and $\text{Var}(G) = \sigma_G^2$ and correlation $\rho = \frac{\mathbb{E}[ZG]}{\sigma_Z \sigma_G}$. Then*

$$\mathbb{E}[\text{sign}(Z)G] = \rho \sigma_G \sqrt{\frac{2}{\pi}}$$

Proof. Define the standardized variables as:

$$U := \frac{Z}{\sigma_Z}, \quad V := \frac{G}{\sigma_G}$$

Then (U, V) is a centered bi-variate Gaussian with

$$\text{Var}(U) = \text{Var}(V) = 1, \quad \rho_{UV} = \text{Corr}(U, V) = \mathbb{E}[UV] = \frac{\mathbb{E}[ZG]}{\sigma_Z \sigma_G} = \rho$$

Thus, (U, V) satisfies the assumptions of Lemma A.12. Applying Lemma A.12 gives:

$$\mathbb{E}[\text{sign}(U)V] = \rho \sqrt{\frac{2}{\pi}}$$

Note that $\text{sign}(U) = \text{sign}(Z)$ since $\sigma_Z > 0$ and $V = \frac{G}{\sigma_G}$. Thus,

$$\begin{aligned} \mathbb{E}[\text{sign}(Z)G] &= \mathbb{E}[\text{sign}(U)\sigma_G V] \\ &= \sigma_G \mathbb{E}[\text{sign}(U)V] \\ &= \rho \sigma_G \sqrt{\frac{2}{\pi}} \end{aligned}$$

□

With these tools in place, we can now analyze each contribution δ_t^i , $i \in \{1, 2, 3\}$ to the feature increment ΔZ_B^t in turn.

A.3. Scaling of Per-Step Update Terms

Recall from Eq. (2) that the per-step LoRA feature increment decomposes into three contributions. In this part we derive the asymptotic scaling of each term for a fixed step t , expressed in terms of the learning rate η , LoRA multiplier α , network width n , rank r , and the current scales of A_{t-1} and B_{t-1} .

Lemma A.14 (Asymptotic Dynamics of δ_t^1). *For t fixed, the asymptotic dynamics of δ_t^1 follows the following formula:*

$$\delta_t^1 = \Theta(\eta \alpha n) \cdot \Theta\left(\sqrt{r + \frac{2}{\pi} \cdot \frac{r(r-1)}{n}}\right) \cdot \Theta(B_{t-1}) \quad (7)$$

Proof. Substituting $\Delta Z_A^t = -\eta g_A^t \underline{Z}$ into δ_t^1 , we have:

$$\begin{aligned} \delta_t^1 &= \alpha B_{t-1} \Delta Z_A^t \\ &= \alpha B_{t-1} \left(-\eta \cdot \text{sign}\left(\frac{\partial \mathcal{L}_t}{\partial A_{t-1}}\right) \underline{Z}\right) \\ &= (-\eta \alpha) \cdot (\text{sign}(\underline{Z})^\top \underline{Z}) \cdot B_{t-1} \cdot \text{sign}(\alpha B_{t-1}^\top d\bar{Z}^{t-1}) \end{aligned}$$

Here, we analyze $B_{t-1} \cdot \text{sign}(\alpha B_{t-1}^\top d\bar{Z}^{t-1})$. For the ease of analysis, we drop the subscript in B_{t-1} and instead use B with $B = \Theta(\beta)$. In addition, we use $h = \alpha d\bar{Z}^{t-1} \in \mathbb{R}^n$ with $\Theta(h) = \Theta(\alpha)$. Let $X = B \cdot \text{sign}(B^\top h)$, we aim to analyze the asymptotic dynamic of X by taking an arbitrary element X_k and analyze $\mathbb{E}[X_k^2]$. To simplify the analysis, we treat $B \in \mathbb{R}^{n \times r}$ as an i.i.d. Gaussian matrix with entries $B_{ij} \stackrel{\text{i.i.d.}}{\sim} \mathcal{N}(0, \beta^2)$, and we assume $h \in \mathbb{R}^n$ is independent of B with entries $h_i \stackrel{\text{i.i.d.}}{\sim} \mathcal{N}(0, \alpha^2)$.

Fixing an index k , we have:

$$X_k = \sum_{a=1}^r B_{ka} \cdot \text{sign}(u_a)$$

where $u_a = \sum_{j=1}^n B_{ja} h_j$. Then we have:

$$\begin{aligned} \mathbb{E}[X_k^2] &= \mathbb{E}\left[\sum_{a=1}^r B_{ka}^2 \text{sign}(u_a)^2 + 2 \sum_{a < a'} B_{ka} \text{sign}(u_a) B_{ka'} \text{sign}(u_{a'})\right] \\ &= r\beta^2 + 2 \sum_{a < a'} \mathbb{E}[B_{ka} \text{sign}(u_a) B_{ka'} \text{sign}(u_{a'})] \end{aligned}$$

Given h , the pair (u_a, B_{ka}) is Gaussian with $\mathbb{E}[u_a | h] = 0$ and $\mathbb{E}[B_{ka} | h] = 0$, and the correlation is

$$\begin{aligned} \rho_k &= \text{Corr}(B_{ka}, u_a | h) \\ &= \frac{\mathbb{E}[B_{ka} u_a | h]}{\sqrt{\text{Var}[B_{ka} | h] \text{Var}[u_a | h]}} \\ &= \frac{h_k \beta^2}{\sqrt{\beta^2 \cdot (\sum_{j=1}^n h_j^2 \beta^2)}} \\ &= \frac{h_k}{\sqrt{\sum_{j=1}^n h_j^2}} \end{aligned}$$

Using Corollary A.13, we have

$$\begin{aligned} \mu &:= \mathbb{E}[B_{ka} \text{sign}(u_a) | h] \\ &= \rho_k \beta \sqrt{\frac{2}{\pi}} \end{aligned}$$

By the same argument, $\mathbb{E}[B_{ka'} \text{sign}(u_{a'}) | h] = \rho_k \beta \sqrt{\frac{2}{\pi}}$. Moreover, conditionally on h , the random variables $B_{ka} \text{sign}(u_a)$ and $B_{ka'} \text{sign}(u_{a'})$ are independent for $a \neq a'$, since they depend on distinct columns of B . This yields:

$$\mathbb{E}[B_{ka} \text{sign}(u_a) B_{ka'} \text{sign}(u_{a'}) | h] = \rho_k^2 \beta^2 \frac{2}{\pi}$$

Therefore,

$$\mathbb{E}[B_{ka} \text{sign}(u_a) B_{ka'} \text{sign}(u_{a'})] = \beta^2 \frac{2}{\pi} \mathbb{E}[\rho_k^2]$$

Denote $h_k = \alpha q_k$ for all k where $q_k \stackrel{\text{iid}}{\sim} \mathcal{N}(0, 1)$, then we have:

$$\mathbb{E}[\rho_k^2] = \mathbb{E}\left[\frac{q_k^2}{\sum_{j=1}^n q_j^2}\right]$$

Let $S = \sum_{j=1}^n q_j^2$. Given that q_j are independent, standard normal random variables, we get $S \sim \chi^2(n)$. Furthermore, by symmetry, we have:

$$\sum_{k=1}^n \mathbb{E}\left[\frac{q_k^2}{S}\right] = \mathbb{E}\left[\frac{\sum_{k=1}^n q_k^2}{S}\right] = 1$$

Therefore, $\mathbb{E}[\rho_k^2] = \frac{1}{n}$, and we obtain:

$$\mathbb{E}[B_{ka} \operatorname{sign}(u_a) B_{ka'} \operatorname{sign}(u_{a'})] = \beta^2 \cdot \frac{2}{\pi} \cdot \frac{1}{n}$$

Plugging this term:

$$\begin{aligned} \mathbb{E}[X_k^2] &= r\beta^2 + 2 \sum_{a < a'} \mathbb{E}[B_{ka} \operatorname{sign}(u_a) B_{ka'} \operatorname{sign}(u_{a'})] \\ &= r\beta^2 + 2 \cdot \frac{r(r-1)}{2} \cdot \beta^2 \cdot \frac{2}{\pi} \cdot \frac{1}{n} \\ &= \beta^2 \left(r + \frac{2}{\pi} \cdot \frac{r(r-1)}{n} \right) \end{aligned}$$

Hence, $X_k = \sqrt{\mathbb{E}[X_k^2]} = \Theta(\beta) \cdot \Theta\left(\sqrt{r + \frac{2}{\pi} \cdot \frac{r(r-1)}{n}}\right)$. Combining things together, we get

$$\begin{aligned} \delta_t^1 &= \Theta(-\eta\alpha) \cdot \Theta(n) \cdot \Theta(B_{t-1}) \cdot \Theta\left(\sqrt{r + \frac{2}{\pi} \cdot \frac{r(r-1)}{n}}\right) \\ &= \Theta(\eta\alpha n) \cdot \Theta(B_{t-1}) \cdot \Theta\left(\sqrt{r + \frac{2}{\pi} \cdot \frac{r(r-1)}{n}}\right) \end{aligned}$$

□

Remark A.15 (Simplified Dynamics for δ_t^1). When $r \leq n$, Lemma A.14 reduces to

$$\delta_t^1 = \Theta(\eta\alpha n\sqrt{r}) \cdot \Theta(B_{t-1}). \quad (8)$$

Lemma A.16 (Asymptotic Dynamics of δ_t^2). For t fixed, the asymptotic dynamics of δ_t^2 follows the following formula:

$$\delta_t^2 = \Theta(\eta\alpha r) \cdot \Theta(Z_A^{t-1}) \quad (9)$$

Proof. Substituting $\Delta B_t = -\eta g_B^t$ and $g_B^t = \operatorname{sign}(\frac{\partial \mathcal{L}_t}{\partial B_{t-1}})$ into δ_t^2 , we have:

$$\begin{aligned} \delta_t^2 &= \alpha \Delta B_t Z_A^{t-1} \\ &= \alpha \left(-\eta \cdot \operatorname{sign}\left(\frac{\partial \mathcal{L}_t}{\partial B_{t-1}}\right) \right) Z_A^{t-1} \\ &= (-\eta\alpha) \operatorname{sign}(\alpha d\bar{Z}^{t-1} \otimes Z_A^{t-1}) Z_A^{t-1} \\ &= (-\eta\alpha) (\operatorname{sign}(\alpha d\bar{Z}^{t-1}) \otimes \operatorname{sign}(Z_A^{t-1})) Z_A^{t-1} \\ &= (-\eta\alpha) (\operatorname{sign}(Z_A^{t-1})^\top Z_A^{t-1}) \operatorname{sign}(\alpha d\bar{Z}^{t-1}) \end{aligned}$$

Therefore, we can get the asymptotic behavior of δ_t^2 as:

$$\begin{aligned} \delta_t^2 &= \Theta(-\eta\alpha) \cdot \Theta(r) \cdot \Theta(Z_A^{t-1}) \cdot \Theta(1) \\ &= \Theta(\eta\alpha r) \cdot \Theta(Z_A^{t-1}) \end{aligned}$$

where the extra r comes from the fact that we are summing over r positive terms in $\operatorname{sign}(Z_A^{t-1})^\top Z_A^{t-1}$. □

Lemma A.17 (Asymptotic Dynamics of δ_t^3). For t fixed, the asymptotic dynamics of δ_t^3 follows the following formula:

$$\delta_t^3 = \Theta(\alpha\eta^2 nr^{1/2}) \quad (10)$$

Proof. Substituting $\Delta B_t = -\eta g_B^t$ and $\Delta Z_A^t = -\eta g_A^t \underline{Z}$ into δ_t^3 , we have:

$$\begin{aligned} \delta_t^3 &= \alpha \Delta B_t \Delta Z_A^t \\ &= \alpha \cdot (-\eta g_B^t) \cdot (-\eta g_A^t \underline{Z}) \\ &= (\alpha\eta^2) \cdot \operatorname{sign}(\alpha d\bar{Z}^{t-1} \otimes Z_A^{t-1}) \cdot \operatorname{sign}(\alpha(B_{t-1}^\top d\bar{Z}^{t-1}) \otimes \underline{Z}) \cdot \underline{Z} \\ &= (\alpha\eta^2) \cdot (\operatorname{sign}(\underline{Z})^\top \underline{Z}) \cdot \operatorname{sign}(\alpha d\bar{Z}^{t-1} \otimes Z_A^{t-1}) \cdot \operatorname{sign}(\alpha B_{t-1}^\top d\bar{Z}^{t-1}) \\ &= (\alpha\eta^2) \cdot (\operatorname{sign}(\underline{Z})^\top \underline{Z}) \cdot (\operatorname{sign}(Z_A^{t-1})^\top \operatorname{sign}(\alpha B_{t-1}^\top d\bar{Z}^{t-1})) \cdot \operatorname{sign}(\alpha d\bar{Z}^{t-1}) \end{aligned}$$

Here, we assume that elements in $\text{sign}(Z_A^{t-1})$ and $\text{sign}(\alpha B_{t-1}^\top d\bar{Z}^{t-1})$ are independent. Under this assumption, we have:

$$\text{sign}(Z_A^{t-1})^\top \text{sign}(\alpha B_{t-1}^\top d\bar{Z}^{t-1}) = \Theta(r^{1/2})$$

Therefore, we have:

$$\begin{aligned}\delta_t^3 &= \Theta(\alpha\eta^2) \cdot \Theta(n) \cdot \Theta(r^{1/2}) \cdot \Theta(1) \\ &= \Theta(\alpha\eta^2 nr^{1/2})\end{aligned}$$

□

With the foregoing lemmas established, the proof of the main theorems becomes straightforward: for each initialization scheme, we (i) identify the induced initial scales of (Z_A^0, B_0) , (ii) propagate these scales through Lemma A.11, (iii) plug into Lemma A.14, Lemma A.16, and Lemma A.17, and (iv) derive the learning rate scaling that yields stable, non-vanishing feature updates ΔZ_B^t , i.e., $\Delta Z_B^t = \Theta(1)$.

A.4. Init[A]: Theorems and Corollaries

This section provides the derivations for the Init[A] regime in which A_0 is randomly initialized and $B_0 = 0$. We follow the same structure as the main text: first characterize the scale of ΔZ_B^t , then impose the stable feature learning condition to obtain the learning rate scaling.

Theorem A.18 (Init[A]). *Under Assumptions A.9 and A.10, for any fixed $t \leq T$ with Init[A],*

$$\Delta Z_B^t = \max\{\Theta(\eta\alpha r), \Theta(\eta^2\alpha rn)\}. \quad (11)$$

Proof. With Init[A], we have $B_0 = 0$ and $Z_A^0 = A_0 \mathbb{Z} = \Theta(1)$. Thus, for all t , we have:

$$\begin{aligned}Z_A^t &= \max(\Theta(1), \Theta(\eta n)) \\ B_t &= \Theta(\eta)\end{aligned}$$

Thus, we have:

$$\begin{aligned}\delta_t^1 &= \Theta(\eta^2\alpha n) \cdot \Theta\left(\sqrt{r + \frac{2}{\pi} \cdot \frac{r(r-1)}{n}}\right) \\ &= \Theta(\eta^2\alpha nr^{1/2}) \\ \delta_t^2 &= \Theta(\eta\alpha r) \cdot \max(\Theta(1), \Theta(\eta n)) \\ &= \max(\Theta(\eta\alpha r), \Theta(\eta^2\alpha rn)) \\ \delta_t^3 &= \Theta(\alpha\eta^2 nr^{1/2})\end{aligned}$$

Therefore,

$$\begin{aligned}\Delta Z_B^t &= \max(\Theta(\delta_t^1), \Theta(\delta_t^2), \Theta(\delta_t^3)) \\ &= \max(\Theta(\eta^2\alpha r^{1/2}n), \Theta(\eta\alpha r), \Theta(\eta^2\alpha rn)) \\ &= \max(\Theta(\eta\alpha r), \Theta(\eta^2\alpha rn))\end{aligned}$$

□

Imposing $\Delta Z_B^t = \Theta(1)$ and solving for the learning rate scaling in terms of (n, r) and $\alpha = r^{-\gamma}$ with $\gamma \in [0, 1]$ yields the following unified scaling laws for Init[A]:

Corollary A.19 (Unified scaling rules for Init[A]). *Let $\alpha = r^{-\gamma}$ for $\gamma \in [0, 1]$. Under Init[A], achieving stable feature learning (i.e., $\Delta Z_B^t = \Theta(1)$ for fixed $t \leq T$) requires*

$$\eta = \Theta(n^{-1/2}r^{-(1-\gamma)/2}).$$

With this choice,

$$\begin{aligned}\delta_t^1 &= \Theta(r^{-1/2}), \\ \delta_t^2 &= \Theta(1), \\ \delta_t^3 &= \Theta(r^{-1/2}),\end{aligned}$$

and the intermediate feature scales as

$$\Theta(Z_A^t) = \Theta(n^{1/2} r^{-(1-\gamma)/2}).$$

In particular:

γ	α	$\Theta(\eta)$	$\Theta(Z_A^t)$
0	1	$n^{-1/2} r^{-1/2}$	$n^{1/2} r^{-1/2}$
$\frac{1}{2}$	$r^{-1/2}$	$n^{-1/2} r^{-1/4}$	$n^{1/2} r^{-1/4}$
1	r^{-1}	$n^{-1/2}$	$n^{1/2}$

Proof. From Equation (11), under Init[A] we have

$$\Delta Z_B^t = \max(\Theta(\eta\alpha r), \Theta(\eta^2\alpha r n)).$$

Substituting $\alpha = r^{-\gamma}$ yields

$$\Delta Z_B^t = \max(\Theta(\eta r^{1-\gamma}), \Theta(\eta^2 n r^{1-\gamma})).$$

To achieve $\Delta Z_B^t = \Theta(1)$, we require

$$\eta = \min\left(\Theta(r^{-(1-\gamma)}), \Theta(n^{-1/2} r^{-(1-\gamma)/2})\right).$$

Since $r \leq n$, we have $r^{-(1-\gamma)} \geq n^{-1/2} r^{-(1-\gamma)/2}$ for all $\gamma \in [0, 1]$. Thus,

$$\eta = \Theta(n^{-1/2} r^{-(1-\gamma)/2}).$$

Feature update terms. Substituting into the expressions from Lemmas A.14, A.16, A.17:

- From Lemma A.14 with $B_{t-1} = \Theta(\eta) = \Theta(n^{-1/2} r^{-(1-\gamma)/2})$:

$$\begin{aligned}\delta_t^1 &= \Theta(\eta\alpha n\sqrt{r}) \cdot \Theta(B_{t-1}) \\ &= \Theta(n^{-1/2} r^{-(1-\gamma)/2} \cdot r^{-\gamma} \cdot n \cdot r^{1/2} \cdot n^{-1/2} r^{-(1-\gamma)/2}) \\ &= \Theta(r^{-1/2}).\end{aligned}$$

- From Lemma A.16, using $Z_A^{t-1} = \max(\Theta(1), \Theta(\eta n)) = \Theta(\eta n)$:

$$\begin{aligned}\delta_t^2 &= \Theta(\eta\alpha r) \cdot \Theta(Z_A^{t-1}) \\ &= \Theta(n^{-1/2} r^{-(1-\gamma)/2} \cdot r^{-\gamma} \cdot r \cdot n^{-1/2} r^{-(1-\gamma)/2} \cdot n) \\ &= \Theta(1).\end{aligned}$$

- From Lemma A.17, we have:

$$\begin{aligned}\delta_t^3 &= \Theta(\alpha\eta^2 n r^{1/2}) \\ &= \Theta(r^{-\gamma} \cdot n^{-1} r^{-(1-\gamma)} \cdot n \cdot r^{1/2}) \\ &= \Theta(r^{-1/2}).\end{aligned}$$

Thus, under Init[A], the dominant contribution comes from δ_t^2 , while δ_t^1 and δ_t^3 vanish as rank $r \rightarrow \infty$.

Intermediate features. From the recursive formula (Lemma A.11):

$$Z_A^t = \max(\Theta(1), \Theta(\eta n)) = \Theta(\eta n) = \Theta(n^{1/2} r^{-(1-\gamma)/2}).$$

□

A.5. Init[B]: Theorems and Corollaries

This part deals with Init[B], in which B_0 is randomly initialized and $A_0 = 0$. As in the main text, we first establish the scale of ΔZ_B^t and then specialize to common multiplier configurations, namely $\alpha = 1$ and $\alpha = r^{-1}$.

Theorem A.20 (Init[B]). *Under Assumptions A.9 and A.10, for any fixed $t \leq T$ with Init[B],*

$$\Delta Z_B^t = \max\{\Theta(\eta\alpha n), \Theta(\eta^2\alpha nr)\}. \quad (12)$$

Proof. With Init[B], we have $B_0 = \Theta(r^{-1/2})$ and $Z_A^0 = 0$. As a result, we have for all $t \leq T$:

$$\begin{aligned} Z_A^t &= \Theta(\eta n) \\ B_t &= \max\left(\Theta(r^{-1/2}), \Theta(\eta)\right) \end{aligned}$$

Thus, we have:

$$\begin{aligned} \delta_t^1 &= \Theta(\eta\alpha nr^{1/2}) \cdot \Theta(B_{t-1}) \\ &= \max\left(\Theta(\eta\alpha n), \Theta(\eta^2\alpha nr^{1/2})\right) \\ \delta_t^2 &= \Theta(\eta^2\alpha nr) \\ \delta_t^3 &= \Theta(\alpha\eta^2nr^{1/2}) \end{aligned}$$

Therefore,

$$\begin{aligned} \Delta Z_B^t &= \max\left(\Theta(\delta_t^1), \Theta(\delta_t^2), \Theta(\delta_t^3)\right) \\ &= \max\left(\Theta(\eta\alpha n), \Theta(\eta^2\alpha nr)\right) \end{aligned}$$

□

We proceed by considering the LoRA multiplier α case by case. We first consider the choice $\alpha = 1$ (Corollary A.21), and then the rank-dependent choice $\alpha = r^{-1}$ (Corollary A.22).

Corollary A.21 (Init[B] with $\alpha = 1$). *Let $\alpha = 1$. Under Init[B], achieving stable feature learning (i.e., $\Delta Z_B^t = \Theta(1)$ for fixed $t \leq T$) requires*

$$\eta = \Theta(n^{-1}).$$

With this choice,

$$\begin{aligned} \delta_t^1 &= \Theta(1), \\ \delta_t^2 &= \Theta(rn^{-1}), \\ \delta_t^3 &= \Theta(r^{1/2}n^{-1}), \end{aligned}$$

and the intermediate feature scales as

$$\Theta(Z_A^t) = \Theta(1).$$

Proof. From Equation (12) with constant α :

$$\Delta Z_B^t = \max\left(\Theta(\eta n), \Theta(\eta^2 nr)\right).$$

Obtaining $\Delta Z_B^t = \Theta(1)$ requires:

$$\eta = \min\left(\Theta(n^{-1}), \Theta(n^{-1/2}r^{-1/2})\right).$$

Since $r \leq n$ implies $n^{-1} \leq n^{-1/2}r^{-1/2}$, we have $\eta = \Theta(n^{-1})$.

Feature update terms. Under Init[B], we have $B_{t-1} = \max(\Theta(r^{-1/2}), \Theta(\eta)) = \Theta(r^{-1/2})$ and $Z_A^{t-1} = \Theta(\eta n) = \Theta(1)$. Substituting into Lemmas A.14, A.16, A.17:

$$\begin{aligned}\delta_t^1 &= \Theta(\eta \alpha n \sqrt{r}) \cdot \Theta(B_{t-1}) \\ &= \Theta(n^{-1} \cdot 1 \cdot n \cdot r^{1/2} \cdot r^{-1/2}) \\ &= \Theta(1), \\ \delta_t^2 &= \Theta(\eta \alpha r) \cdot \Theta(Z_A^{t-1}) \\ &= \Theta(n^{-1} \cdot r \cdot 1), \\ &= \Theta(r n^{-1}) \\ \delta_t^3 &= \Theta(\alpha n^2 n r^{1/2}) \\ &= \Theta(1 \cdot n^{-2} \cdot n \cdot r^{1/2}) \\ &= \Theta(r^{1/2} n^{-1}).\end{aligned}$$

Intermediate features. From the recursive formula (Lemma A.11):

$$\begin{aligned}Z_A^t &= \Theta(\eta n) \\ &= \Theta(1)\end{aligned}$$

□

Corollary A.22 (Init[B] with $\alpha = r^{-1}$). *Let $\alpha = r^{-1}$. Under Init[B], achieving stable feature learning (i.e., $\Delta Z_B^t = \Theta(1)$ for fixed $t \leq T$) requires*

$$\eta = \min \left(\Theta(r n^{-1}), \Theta(n^{-1/2}) \right). \quad (13)$$

With this choice, the feature update terms satisfy:

$$\begin{aligned}\delta_t^1 &= \Theta(\eta n r^{-1}) \\ \delta_t^2 &= \Theta(\eta^2 n) \\ \delta_t^3 &= \Theta(\eta^2 n r^{-1/2})\end{aligned}$$

and the intermediate feature scales as

$$Z_A^t = \Theta(\eta n)$$

In particular:

- If $r \leq \sqrt{n}$, we have $\eta = \Theta(r n^{-1})$ and thus obtain:

$$\begin{aligned}\delta_t^1 &= \Theta(1) \\ \delta_t^2 &= \Theta(r^2 n^{-1}) \\ \delta_t^3 &= \Theta(r^{3/2} n^{-1}) \\ Z_A^t &= \Theta(r)\end{aligned}$$

- If $r > \sqrt{n}$, we have $\eta = \Theta(n^{-1/2})$ and thus obtain:

$$\begin{aligned}\delta_t^1 &= \Theta(n^{1/2} r^{-1}) \\ \delta_t^2 &= \Theta(1) \\ \delta_t^3 &= \Theta(r^{-1/2}) \\ Z_A^t &= \Theta(n^{1/2}).\end{aligned}$$

Proof. Substituting $\alpha = r^{-1}$ into Theorem A.20 gives

$$\begin{aligned}\Delta Z_B^t &= \max(\Theta(\eta\alpha n), \Theta(\eta^2\alpha n r)) \\ &= \max(\Theta(\eta n r^{-1}), \Theta(\eta^2 n)).\end{aligned}$$

Imposing $\Delta Z_B^t = \Theta(1)$ yields

$$\eta = \min\left(\Theta(r n^{-1}), \Theta(n^{-1/2})\right).$$

Feature update terms. Under Init[B], we have $B_{t-1} = \max(\Theta(r^{-1/2}), \Theta(\eta)) = \Theta(r^{-1/2})$ for either choice of η and $Z_A^{t-1} = \Theta(\eta n)$. Substituting into Lemmas A.14, A.16, A.17:

$$\begin{aligned}\delta_t^1 &= \Theta(\eta\alpha n\sqrt{r}) \cdot \Theta(B_{t-1}) \\ &= \Theta(\eta n r^{-1}), \\ \delta_t^2 &= \Theta(\eta\alpha r) \cdot \Theta(Z_A^{t-1}) \\ &= \Theta(\eta^2 n), \\ \delta_t^3 &= \Theta(\alpha\eta^2 n r^{1/2}) \\ &= \Theta(\eta^2 n r^{-1/2}).\end{aligned}$$

Next, we need to consider the relationship between the network width n and the LoRA rank r to determine scaling rule of η .

When $r \leq \sqrt{n}$, we have $r n^{-1} \leq n^{-1/2}$ and thus $\eta = \Theta(r n^{-1})$, which incurs:

$$\begin{aligned}\delta_t^1 &= \Theta(1) \\ \delta_t^2 &= \Theta(r^2 n^{-1}) \\ \delta_t^3 &= \Theta(r^{3/2} n^{-1})\end{aligned}$$

When $r > \sqrt{n}$, we have $r n^{-1} > n^{-1/2}$ and thus $\eta = \Theta(n^{-1/2})$, which incurs:

$$\begin{aligned}\delta_t^1 &= \Theta(n^{1/2} r^{-1}) \\ \delta_t^2 &= \Theta(1) \\ \delta_t^3 &= \Theta(r^{-1/2})\end{aligned}$$

Intermediate features. From the recursive formula (Lemma A.11):

$$Z_A^t = \Theta(\eta n)$$

Similarly, when $r \leq \sqrt{n}$, we have:

$$Z_A^t = \Theta(r)$$

When $r > \sqrt{n}$, we obtain:

$$Z_A^t = \Theta(n^{1/2})$$

□

A.6. Learning Rate Scaling for Full Finetuning

In this section, we analyze how the learning rate should scale for full finetuning with regard to the network width n . We use a framework similar to our previous derivations.

Consider a single linear layer of width n and pretrained weights $W^* \in \mathbb{R}^{n \times n}$. Under full finetuning, we update W directly. Here we denote the per-step weight update by

$$\Delta W_t := W_t - W_{t-1}, \quad W_0 := W^*.$$

Then, for any fixed $t \leq T$, the layer output can be written as

$$\bar{Z}^t = W_t \underline{Z} = W^* \underline{Z} + \sum_{s=1}^t \Delta W_s \underline{Z}. \quad (14)$$

Following Assumption A.9, we assume that pretraining yields bounded features $\underline{Z} = \mathcal{O}(1)$ and $W^* \underline{Z} = \mathcal{O}(1)$. By Lemma A.6, it suffices to control each per-step increment $\Delta W_s \underline{Z}$ for feature stability: requiring $\Delta W_s \underline{Z} = \mathcal{O}(1)$ for all $s \leq t$ implies $\sum_{s=1}^t \Delta W_s \underline{Z} = \mathcal{O}(1)$. To avoid vanishing updates, we also impose $\Delta W_s \underline{Z} = \Theta(1)$. Assuming that we are using SignSGD (Assumption A.10) and single-sample loss, we can obtain the following theorem:

Theorem A.23 (Scaling rules for full finetuning). *Under Assumptions A.9 and A.10, for any fixed $t \leq T$, with full finetuning, the learning rate should scale as*

$$\eta = \Theta(n^{-1}). \quad (15)$$

Proof. Under SignSGD, the per-step update is $\Delta W_t = -\eta g_t$, where

$$g_t := \text{sign}\left(\frac{\partial \mathcal{L}_t}{\partial W_{t-1}}\right).$$

For the linear map $\bar{Z} = W \underline{Z}$, the gradient factorizes as:

$$\frac{\partial \mathcal{L}_t}{\partial W_{t-1}} = d\bar{Z}^{t-1} \otimes \underline{Z}, \quad (16)$$

where $d\bar{Z}^{t-1} := \partial \mathcal{L}_t / \partial \bar{Z}^{t-1}$ and \otimes denotes the outer product. Therefore,

$$\begin{aligned} \Delta W_t &= -\eta \text{sign}(d\bar{Z}^{t-1} \otimes \underline{Z}) \\ &= -\eta (\text{sign}(d\bar{Z}^{t-1}) \otimes \text{sign}(\underline{Z})). \end{aligned}$$

Multiplying by \underline{Z} yields

$$\Delta W_t \underline{Z} = \Theta(\eta \cdot (\text{sign}(\underline{Z})^\top \underline{Z}) \cdot \text{sign}(d\bar{Z}^{t-1})) \quad (17)$$

$$= \Theta(\eta n), \quad (18)$$

since $\text{sign}(\underline{Z})^\top \underline{Z} = \|\underline{Z}\|_1 = \Theta(n)$ and $\text{sign}(\cdot) = \Theta(1)$. Imposing $\Delta W_t \underline{Z} = \Theta(1)$ yields:

$$\eta = \Theta(n^{-1}).$$

□

From above, we show that under the same assumptions, full finetuning admits the *same* width-dependent learning rate scaling $\eta = \Theta(n^{-1})$. At the same time, our analysis for LoRA with Init[B] and constant $\alpha = 1$ shows that stable (non-exploding) and non-vanishing feature updates require a learning rate $\eta = \Theta(n^{-1})$ (Corollary A.21). This matching of learning rate scaling might indicate that the hyperparameter landscapes of full finetuning and LoRA with Init[B] and constant $\alpha = 1$ are very close, which opens up an opportunity to do learning rate transfer between these two regimes.

Table 2. Shared optimization and training settings.

Setting	Value
Optimizer	AdamW [56]
AdamW momentum	$\beta_1 = 0.9, \beta_2 = 0.999$
AdamW epsilon	$\epsilon = 10^{-8}$
Weight decay	0.01
Gradient clipping	global norm clipped to 1.0
LR schedule	linear warmup for first 5% of steps, then cosine decay to $0.1 \times$ peak LR
Precision	bfloat16 mixed precision; TF32 matmul enabled
LoRA dropout	0.0
LoRA Bias	None

B. Implementation and Experimental Details

In this section, we provide more details on our experimental settings.

B.1. Model Configuration

All pretrained models are obtained from public model hubs and used without architectural modifications beyond (i) adding LoRA adapters and (ii) adding a linear classification head for discriminative tasks. Concretely, we use the following models:

- **Llama-3.2-1B** [18] (meta-llama/Llama-3.2-1B)².
- **Qwen2.5-3B-Instruct** [64] (Qwen/Qwen2.5-3B-Instruct)³.
- **RoBERTa-large** [55] (FacebookAI/roberta-large)⁴.
- **ViT-Huge/14** [15] (google/vit-huge-patch14-224-in21k)⁵.
- **Qwen3-VL-2B-Instruct** [1] (Qwen/Qwen3-VL-2B-Instruct)⁶.
- **Stable Diffusion v1.5** [69]. We use the standard *v1.5* weights in diffusers format; a widely used public mirror is stable-diffusion-v1-5/stable-diffusion-v1-5⁷.
- **Llama-3.1-8B** [18] (meta-llama/Llama-3.1-8B)⁸.

For discriminative tasks, we attach a task-specific classification head to the final pooled representation: the pooled text representation for RoBERTa on ANLI, and the [CLS] token embedding for ViT on ImageNet-1K. During training, this classification head is trained jointly with either the full backbone (full finetuning) or the adapters (LoRA). Across all hyperparameter sweeps, we fix the classifier learning rate at 10^{-3} and only vary the backbone (or adapter) learning rate.

Unless otherwise mentioned, we use the same optimizer and learning rate schedule across all architectures. The random seed is set to 42 across all experiments. Table 2 summarizes these settings.

B.2. LoRA Configurations and PEFT Implementation

Throughout the paper, we analyze the LoRA-augmented weight matrix formulated as follows:

$$\mathbf{W} \leftarrow \mathbf{W} + \alpha \mathbf{B} \mathbf{A},$$

²<https://huggingface.co/meta-llama/Llama-3.2-1B>

³<https://huggingface.co/Qwen/Qwen2.5-3B-Instruct>

⁴<https://huggingface.co/FacebookAI/roberta-large>

⁵<https://huggingface.co/google/vit-huge-patch14-224-in21k>

⁶<https://huggingface.co/Qwen/Qwen3-VL-2B-Instruct>

⁷<https://huggingface.co/stable-diffusion-v1-5/stable-diffusion-v1-5>

⁸<https://huggingface.co/meta-llama/Llama-3.1-8B>

Table 3. Implementation details of LoRA placement across different models, based on the PEFT package. For vision-language models, we use regular expressions to identify target modules. For the diffusion model, we apply LoRA only to the U-Net denoiser.

Models	Target Modules
Decoder-only LMs (Llama, Qwen2.5)	gate_proj, up_proj, down_proj
Encoder-only models (RoBERTa, ViT)	query, key, value attention.output.dense, intermediate.dense, output.dense
Vision-language model (Qwen3-VL)	model.visual.blocks.\d+.attn.qkv model.visual.blocks.\d+.attn.proj model.visual.blocks.\d+.mlp.linear_fc[12] model.visual.merger.linear_fc[12] model.visual.deepstack_merger_list.\d+.linear_fc[12] model.language_model.layers.\d+.mlp.gate_proj model.language_model.layers.\d+.mlp.up_proj model.language_model.layers.\d+.mlp.down_proj
Diffusion (Stable Diffusion v1.5)	to_k, to_q, to_v, to_out.0

where $\mathbf{A} \in \mathbb{R}^{r \times n}$ and $\mathbf{B} \in \mathbb{R}^{n \times r}$ are rank- r factors, and α is the LoRA multiplier.

Our implementation uses the PEFT library [57], which internally parameterizes the update as

$$\mathbf{W} \leftarrow \mathbf{W} + \frac{s}{r} \mathbf{B} \mathbf{A},$$

where s corresponds to `lora_alpha` in `LoraConfig`. To achieve an effective multiplier α in our notation, we set $s = \alpha r$. For example, constant multiplier $\alpha = 1$ requires `lora_alpha = r`, whereas rank-dependent multiplier $\alpha = r^{-1}$ requires `lora_alpha = 1`. In both cases, we set `use_rslora=False`.

We study the three LoRA configurations described in Section 5.1:

- **Init[A] with $\alpha = 1$:** initialize \mathbf{A} randomly and set $\mathbf{B} = \mathbf{0}$. Set `lora_alpha` to the rank used.
- **Init[A] with $\alpha = r^{-1}$:** same initialization as above, but use a multiplier $\alpha = r^{-1}$. Set `lora_alpha` to 1.
- **Init[B] with $\alpha = 1$:** initialize \mathbf{B} randomly and set $\mathbf{A} = \mathbf{0}$. Set `lora_alpha` to the rank used.

In all cases, the *effective* update at initialization is exactly zero (because one factor is initialized to zero), so the LoRA-augmented model initially matches the pretrained backbone. For the nonzero factor, we use Kaiming normal initialization [32]. In terms of the per-entry variance, this corresponds to $\text{Var}(A_{ij}) = 1/n$ for Init[A] and $\text{Var}(B_{ij}) = 1/r$ for Init[B], matching the theoretical definition in Definition 3.2.

Where LoRA is applied. As listed in Table 3, our adapter placement strategy is:

- **Decoder-only LMs (Llama, Qwen2.5):** LoRA is inserted *only* into the feed-forward (MLP) block of each transformer layer (i.e., the expansion, gating, and contraction projections of the MLP).
- **Encoder-only models (RoBERTa, ViT):** LoRA is inserted into all linear projections within each attention block (query/key/value/output) and within the feed-forward block (the two MLP linear layers).
- **Vision-language model (Qwen3-VL):** LoRA is inserted into (i) the vision encoder linear projections, (ii) the vision-language merger module (the “merger” MLP), and (iii) the text decoder *MLP blocks*.
- **Diffusion (Stable Diffusion v1.5):** LoRA is inserted into all self-attention and cross-attention linear projections (query/key/value/output) in the denoising U-Net. The variational autoencoder (VAE) [41] and the CLIP text encoder [66] remain frozen.

Table 4. Task-specific settings used in our experiments. Effective batch size refers to the number of examples (or fixed-length packed blocks) processed per optimizer step, accounting for gradient accumulation. Input size refers to maximum sequence length for language tasks, image resolution for vision tasks, and maximum generation length for RVLVR task; this field is omitted for vision–language tasks. NLL stands for negative log-likelihood, while FID stands for Fréchet Inception Distance.

Model	Dataset	Train / Val size	Input size	Effective batch size	Validation metric
Llama-3.2-1B	Tulu-3 SFT mixture	320k / 32k	1024	32	Token-level NLL
Qwen2.5-3B-Instruct	OpenThoughts-114k	71k / 6k	8192	8	Token-level NLL
RoBERTa-large	ANLI	163k / 3k	128	32	Accuracy
ViT-Huge/14	ImageNet-1K	1.28M / 50k	224 × 224	512	Top-1 accuracy
Qwen3-VL-2B-Instruct	LLaVA-Instruct-Mix	198k / 17k	-	32	Token-level NLL
Stable Diffusion v1.5	Naruto-BLIP-Captions	1.1k / 0.1k	512 × 512	8	FID scores
Llama-3.1-8B (RLVR)	GSM8k	500 / 50	1024	8	Test Reward

B.3. Supervised Finetuning Setting

Summary of task-specific settings. Table 4 summarizes the task-level choices that are not fully shared (data sources, input sizing, and the primary validation metric). For datasets without an official validation split, we create a held-out split by reserving 8% of the samples for validation and using the remaining 92% for training.

B.3.1. LANGUAGE MODELING TASKS

Tulu-3 SFT mixture (Llama-3.2-1B). For instruction-following task, we use Llama-3.2-1B [18] trained on the Tulu-3 supervised finetuning mixture [43], available as `allenai/tulu-3-sft-mixture`⁹. The dataset comprises instruction-following conversations formatted as (user prompt, assistant response) pairs. To keep training time per round manageable, we subsample 320k and 32k examples from the original dataset for training and validation, respectively. We truncate sequences to a maximum length of 1024 tokens, and use dynamic padding within each mini-batch. The effective batch size is 32 samples per optimizer step.

OpenThoughts-114k (Qwen2.5-3B-Instruct). To evaluate long-context reasoning, we train Qwen2.5-3B-Instruct [64] on OpenThoughts-114k [19], available as `open-thoughts/OpenThoughts-114k`¹⁰. Each example contains a system instruction and a multi-turn conversation in which assistant messages include both reasoning traces and final answers. For computational tractability, we draw 71k and 6k examples for training and validation, respectively. Since sequence lengths vary widely, we employ fixed-length packing [67]: tokenized conversations are concatenated with end-of-sequence delimiters into blocks of exactly 8192 tokens. To minimize padding overhead, we adopt a padding-free batching strategy that concatenates packed blocks into a single sequence per optimizer step, using attention masking and position indexing to prevent cross-block attention. The effective batch size is 8 packed blocks per step.

B.3.2. ENCODER-BASED CLASSIFICATION TASKS

ANLI (RoBERTa-large). Natural language inference experiments use RoBERTa-large [55] on the Adversarial NLI benchmark [60], available as `facebook/anli`¹¹. We merge all three rounds by concatenating `train_r1`, `train_r2`, and `train_r3` into a single training set, and similarly concatenating `dev_r1`, `dev_r2`, and `dev_r3` into a single validation set. Each example consists of a premise–hypothesis pair, which we encode using the standard RoBERTa sentence-pair format with separator tokens and truncate to a maximum of 128 tokens. We apply dynamic padding within each mini-batch. The model predicts a 3-way classification label (entailment, neutral, or contradiction).

ImageNet-1K (ViT-Huge/14). For large-scale image classification, we adapt ViT-Huge/14 [15] to ImageNet-1K [11], available as `ILSVRC/imagenet-1k`¹², using the standard ILSVRC-2012 training and validation splits (1.28M and 50k

⁹<https://huggingface.co/datasets/allenai/tulu-3-sft-mixture>

¹⁰<https://huggingface.co/datasets/open-thoughts/OpenThoughts-114k>

¹¹<https://huggingface.co/datasets/facebook/anli>

¹²<https://huggingface.co/datasets/ILSVRC/imagenet-1k>

Table 5. Prompt template used in the RLVR experiments, where {QUESTION} is replaced by the problem statement from each example.

Prompt template
<i>Solve the following grade-school math problem. Show reasoning in <think>...</think>, then give the final numerical answer in <answer>...</answer>.</i>
<i>Question: {QUESTION}</i>
<i>Solution:</i>

images, respectively). Images are converted to RGB and resized to 224×224 pixels. During training, we apply standard ImageNet augmentation (random resized crop and horizontal flip with a flipping probability of 0.5); for evaluation, we use deterministic resizing with center cropping. We normalize inputs per channel with mean and standard deviation of 0.5, as specified by the pretrained checkpoint.

B.3.3. VISION–LANGUAGE TASK

LLaVA-Instruct-Mix (Qwen3-VL-2B-Instruct). Vision–language experiments employ Qwen3-VL-2B-Instruct [1] trained on LLaVA-Instruct-Mix, available as `trl-lib/llava-instruct-mix`¹³. Each example pairs a single image with a user prompt and assistant response. To limit compute, we subsample 198k training and 17k validation samples in our experiment. We use the official Qwen3-VL multimodal processor, which encodes images at native resolution with a SigLIP-2 vision encoder [76], compresses 2×2 visual features into a single visual token via an MLP merger, and applies the chat template to interleave visual and text tokens into the final input sequence.

B.4. Reinforcement Learning with Verifiable Rewards (RVLR) Setting

GSM8k (Llama-3.1-8B). We finetune Llama-3.1-8B [18] with reinforcement learning using verifiable, rule-based rewards via Group Relative Policy Optimization (GRPO) [71]. Our experiments use the GSM8k [8] dataset, available as `openai/gsm8k`¹⁴. This dataset contains 8.5k grade-school math problems paired with their solutions. We randomly sample the 500 training problems and 50 test problems for our training and validation splits, respectively. Each problem is converted into a prompt using a template we design to elicit the model’s reasoning; the prompt template is summarized in Table 5. We compute a scalar reward for each sampled completion and sum over two rule-based components:

- *Accuracy reward*: assigns +1 when the extracted final answer matches the reference, and 0 otherwise.
- *Format reward*: assigns +0.1 when the completion places reasoning within `<think>...</think>` tags and the final answer within `<answer>...</answer>` tags, and 0 otherwise.

For each prompt, we sample 8 completions from the current policy using temperature 1.0, with no nucleus truncation ($\text{top-}p = 1.0$), no top- k truncation ($\text{top-}k = 0$), and repetition penalty 1.0. We set the maximum completion length to 1024 tokens and standardize rewards within each prompt’s sample group. We use the DAPO variant [90] of the GRPO loss, which uses a token-level loss to accommodate longer sequences. We set weight decay to 0, as it strongly degraded performance in our experiments. We omit the KL penalty term since it provides minimal benefit while increasing memory overhead by requiring a reference model to be loaded.

B.5. Text-to-image Diffusion Model Finetuning Setting

Naruto-BLIP-Captions (Stable Diffusion v1.5). For text-to-image generation, we adapt Stable Diffusion v1.5 [69] using Naruto-BLIP-Captions [6], available as `lambdalabs/naruto-blip-captions`¹⁵. The dataset contains 1.2k image–caption pairs; we reserve 8% for validation. Images are resized and cropped to 512×512 , then encoded into the latent space of the pretrained VAE [41]. Captions are tokenized using the pretrained CLIP text encoder [66]. During finetuning, we freeze both the VAE and text encoder, tuning only the denoising U-Net. We use the DDPM noise scheduler [34] with

¹³<https://huggingface.co/datasets/trl-lib/llava-instruct-mix>

¹⁴<https://huggingface.co/datasets/openai/gsm8k>

¹⁵<https://huggingface.co/datasets/lambdalabs/naruto-blip-captions>

an epsilon (noise) prediction objective. We train for 10,000 optimizer steps with a batch size of 8. Unlike the supervised finetuning experiments, the denoising loss is not reliably monotonic during LoRA finetuning, so we select the best learning rate based on validation FID.

B.6. Evaluation Protocol and Hyperparameter Sweeps

Metrics. In addition to the training loss, we also report the evaluation metric for each task, summarized in Table 4. These metrics are defined as follows:

- **Token-level negative log-likelihood (NLL)** is computed as the average negative log-probability assigned by the model to each ground-truth token in the sequence. Lower NLL indicates better predictive performance.
- **Accuracy** for ANLI and ImageNet-1K: top-1 classification accuracy on the validation split. Higher is better.
- **Fréchet Inception Distance (FID)** [33] measures the distributional similarity between generated and real images. We extract features from the 2048-dimensional final pooling layer of Inception v3 [73], with images resized to 299×299 . Lower FID indicates higher fidelity to the training data.
- **Reward** for RLVR task: Mean per-completion reward on the held-out GSM8k test subset, averaged over 8 sampled completions per prompt. Each completion receives +1.0 if the extracted final answer matches the reference, and an additional +0.1 if it follows the expected output format.

Table 6. Learning rate sweep ranges ($\log_2 \eta$) for each model and configuration.

Model	Init[A], $\alpha=1$	Init[A], $\alpha=r^{-1}$	Init[B], $\alpha=1$
Llama-3.2-1B	[-17, -9]	[-13, -7]	[-20, -11]
Qwen2.5-3B-Instruct	[-15, -8]	[-11, -7]	[-16, -11]
Qwen3-VL-2B-Instruct	[-17, -9]	[-13, -7]	[-18, -11]
RoBERTa-large	[-18, -8]	[-13, -7]	[-19, -12]
ViT-Huge/14	[-15, -7]	[-11, -5]	[-15, -9]
Stable Diffusion v1.5	[-14, -7]	[-12, -5]	[-14, -7]
Llama-3.1-8B	[-18, -11]	[-16, -11]	[-21, -15]

Learning rate sweep design. We sweep the learning rate on a \log_2 grid (i.e., adjacent points differ by a factor of two). The grid range varies across LoRA configurations, models, and tasks, chosen to span from peak training performance to the onset of divergence. For full finetuning, we choose the same learning rate grid as Init[B] with $\alpha = 1$ for comparison. For language modeling tasks, we report final training loss (EMA-smoothed with a smoothing factor of 0.1) and validation NLL. For classification, we report final training loss (EMA-smoothed) and validation accuracy. For diffusion, we report validation FID. For RLVR tasks, we report final training reward (EMA-smoothed) and test reward. We select the optimal learning rate separately for each metric.

Rank grids. To manage computational cost, we evaluate each configuration over a small grid of LoRA ranks, using 5 ranks in total. For Init[A], we examine how the optimal learning rate scales with rank under different multipliers α and compare the observed trends against our theoretical predictions. To capture behavior across a broad range, we use ranks $r \in \{4, 16, 64, 256, 1024\}$ (increasing by a factor of $4\times$). For Init[B] with $\alpha = 1$, we additionally test our hyperparameter transfer conjecture by comparing its optimal learning rate with that of full finetuning. To verify whether the transfer holds across most ranks within a range, we use a denser grid with $2\times$ steps: $r \in \{16, 32, 64, 128, 256\}$. For RLVR tasks, practitioners typically favor small ranks, with $r = 1$ being commonly used in practice. Therefore, we use $r \in \{1, 4, 16, 64, 256\}$ for both Init[A] and Init[B]. For diffusion model finetuning task, we use $r \in \{1, 4, 16, 64, 256\}$ for Init[A] and keep $r \in \{16, 32, 64, 128, 256\}$ for Init[B].

Learning rate grids. Table 6 lists the learning rate exponent ranges used for each setting. We evaluate every integer exponent in the stated range (i.e., step size of 1). Full finetuning uses the same range as Init[B], $\alpha = 1$.

Table 7. Software packages and versions.

Component	Version
torch [63]	2.7.0+cu128
CUDA toolkit	12.8
transformers [82]	4.57.1
peft [57]	0.17.0
trl [79]	0.26.2
datasets [45]	4.3.0
diffusers [78]	0.36.0
evaluate	0.4.6
torchvision [75]	0.22.0+cu128
torchmetrics [12]	1.8.2
kernels	0.11.7
flash_attn [10]	2.8.3

B.7. Hardware Configuration

All experiments were conducted on a single compute node running Ubuntu 24.04.3 LTS, equipped with two Intel Xeon Gold 6448Y CPUs (64 physical cores total), 1.0 TiB of system memory, and four NVIDIA H200 GPUs (141 GiB HBM each). We used NVIDIA driver version 590.44.01 with CUDA 13.1.

B.8. Software Configuration

Our implementation is based on PyTorch and the Hugging Face ecosystem: `transformers` for model APIs, `peft` for LoRA injection, `trl` for supervised finetuning and reinforcement learning, `diffusers` for Stable Diffusion, `datasets` for data loading, and `evaluate/torchmetrics` for evaluation. We enable mixed-precision training (bf16/TF32 `matmul`), fused AdamW kernels, and FlashAttention-2 [10] implementation. Version details are listed in Table 7.

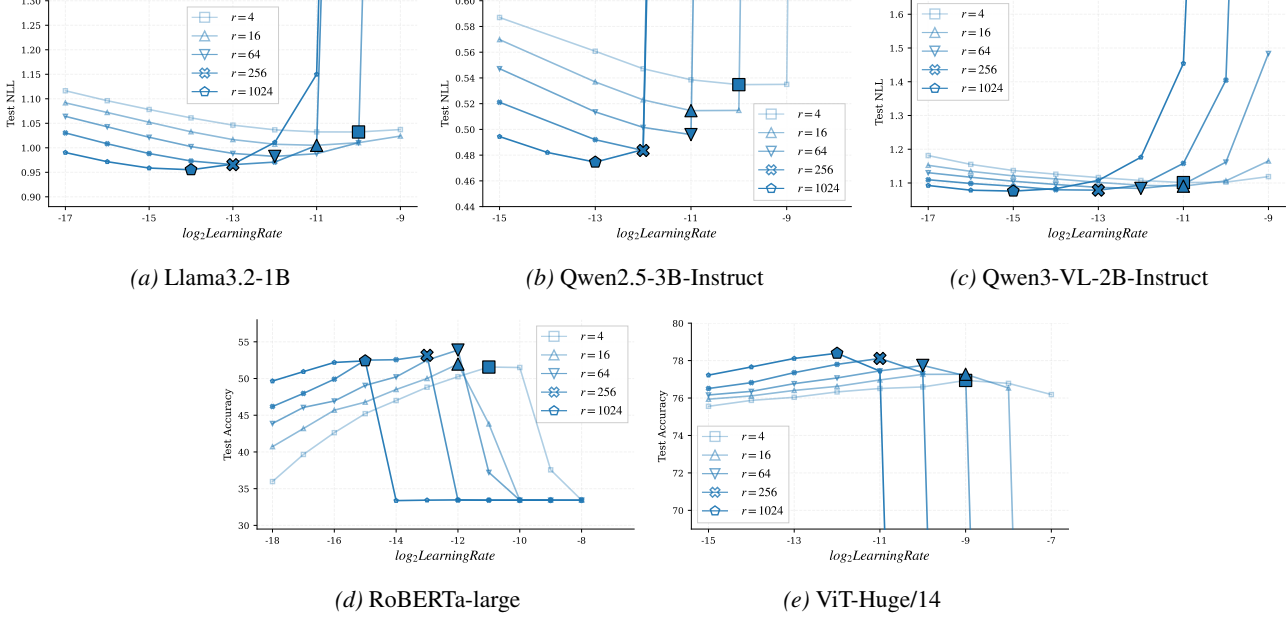


Figure 8. Learning rate sweeps for $\text{Init}[\mathbf{A}]$ with $\alpha = 1$ across five models. Curves show evaluation metrics versus log-scale learning rate $\log_2(\eta)$. Large markers denote per-rank optima. Y-axes are clipped for readability. Top: models finetuned on language modeling tasks, evaluated by test NLL (lower is better). Bottom: models finetuned on classification tasks, evaluated by top-1 accuracy (higher is better).

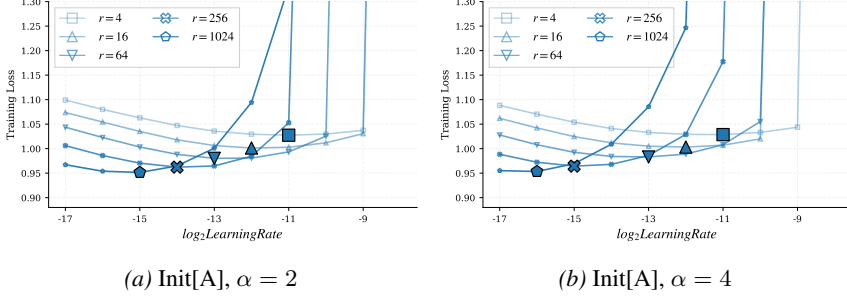


Figure 9. Learning rate sweeps on Llama-3.2-1B (tulu3) for $\text{Init}[\mathbf{A}]$ with (a) $\alpha = 2$ and (b) $\alpha = 4$. Curves show training loss versus log-scale learning rate $\log_2(\eta)$. Large markers indicate the optimal learning rate for each rank.

C. Additional Results for Supervised Finetuning (SFT)

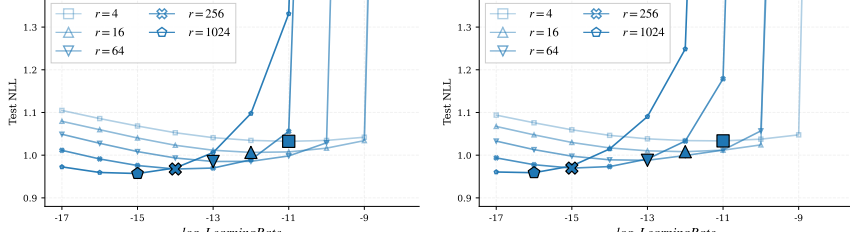
C.1. $\text{Init}[\mathbf{A}]$ with Constant $\alpha = 1$

Figure 8 shows learning rate sweeps for $\text{Init}[\mathbf{A}]$ with $\alpha = 1$, where the optimal learning rate is selected using task-specific validation metrics. We observe a consistent pattern with Figure 3.

Our theory applies when the LoRA multiplier α remains constant as rank r increases. Figure 9 and Figure 10 show that a consistent pattern holds for other constant values such as $\alpha = 2$ and $\alpha = 4$: as rank r increases, the optimal learning rate decreases accordingly.

C.2. $\text{Init}[\mathbf{A}]$ with Rank-Dependent $\alpha = r^{-1}$

Figure 11 shows learning rate sweeps for $\text{Init}[\mathbf{A}]$ with $\alpha = r^{-1}$, where the optimal learning rate is selected using task-specific validation metrics. We observe a consistent pattern with Figure 4.


 (a) Init[A], $\alpha = 2$

 (b) Init[A], $\alpha = 4$

Figure 10. Learning rate sweeps on Llama-3.2-1B (tulu3) for Init[A] with (a) $\alpha = 2$ and (b) $\alpha = 4$. Curves show test loss versus log-scale learning rate $\log_2(\eta)$. Large markers indicate the optimal learning rate for each rank.

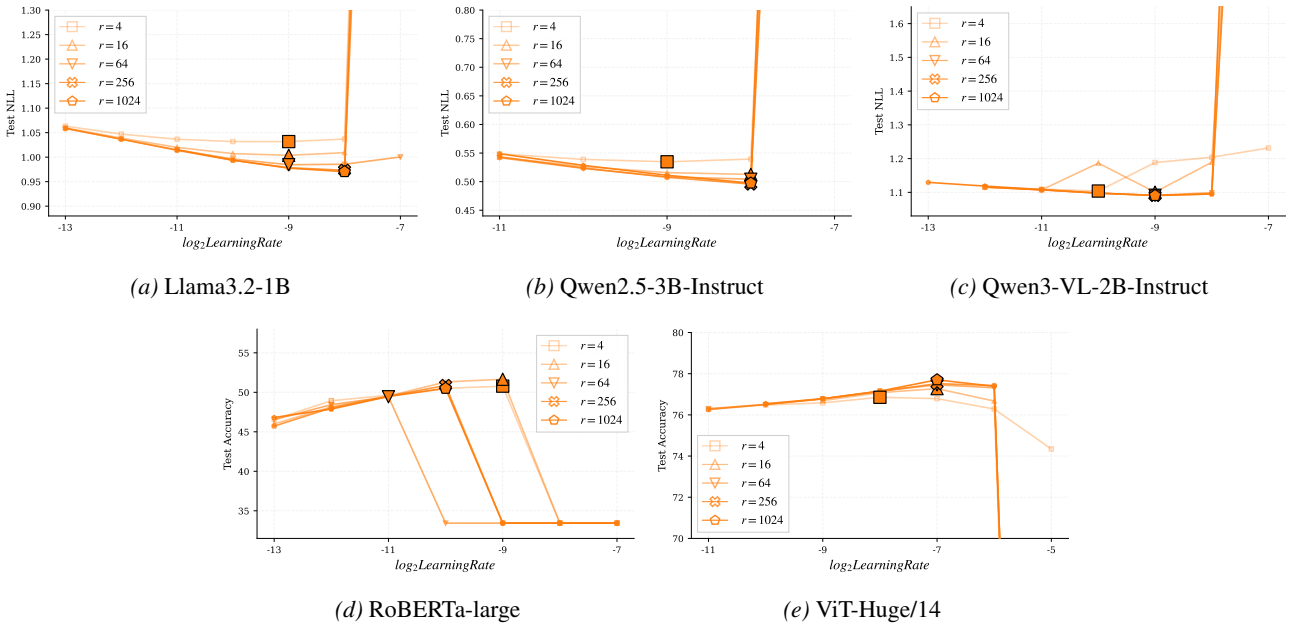


Figure 11. Learning rate sweeps for Init[A] with $\alpha = r^{-1}$ across five models. Curves show evaluation metrics versus log-scale learning rate $\log_2(\eta)$. Large markers denote per-rank optima. Y-axes are clipped for readability. Top: models finetuned on language modeling tasks, evaluated by test NLL (lower is better). Bottom: models finetuned on classification tasks, evaluated by accuracy (higher is better).

C.3. Init[B] with Constant $\alpha = 1$

Figure 12 shows learning rate sweeps for Init[B] with $\alpha = 1$, where the optimal learning rate is selected using task-specific validation metrics. We observe a consistent pattern with Figure 5.

D. Additional Results for Reinforcement Learning with Verifiable Rewards (RLVR)

D.1. Learning Rate Sweep Results

Figure 13 shows learning rate sweeps for Init[A] with $\alpha = r^{-1}$ and Init[B] with $\alpha = 1$, where the optimal learning rate is selected using the test reward. We observe a consistent pattern with Figure 6.

Figure 14 shows the learning rate sweeps for Init[A] with constant $\alpha = 1$ across multiple ranks. The learning rate sweeps reveal patterns consistent with our SFT findings. Under Init[A] with $\alpha = 1$, the optimal learning rate should scale inversely with the square root of the rank: $\eta \propto r^{-1/2}$. In the figure, we observe that as the rank increases, the optimal learning rate decreases accordingly, and this pattern is consistent across both training reward and test reward. Moreover, we observe that the peak performance is comparable across different ranks, consistent with findings in [70].

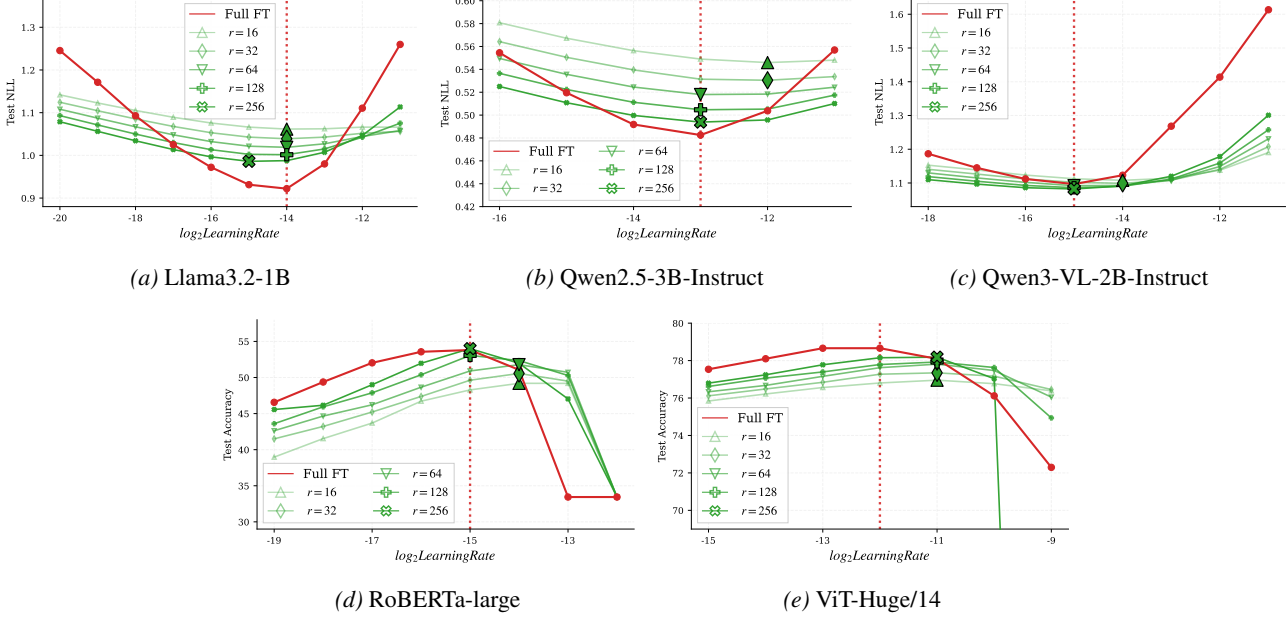


Figure 12. Learning rate sweeps for $\text{Init}[\mathbf{B}]$ with $\alpha = 1$ across five models. Curves show evaluation metrics versus log-scale learning rate $\log_2(\eta)$ for multiple ranks (green) and FFT (red). Large markers denote per-rank optima. Y-axes are clipped for readability. The red vertical dashed line marks the optimal FFT learning rate. Top: models finetuned on language modeling tasks, evaluated by test NLL (lower is better). Bottom: models finetuned on classification tasks, evaluated by top-1 accuracy (higher is better).

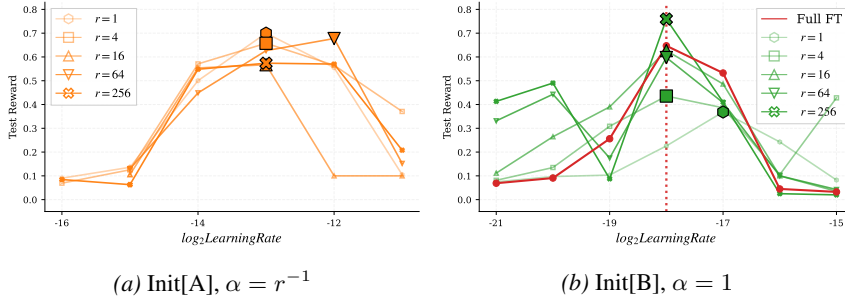


Figure 13. RLVR results on Llama-3.1-8B (GSM8k) for (a) $\text{Init}[\mathbf{A}]$ with $\alpha = r^{-1}$ and (b) $\text{Init}[\mathbf{B}]$ with $\alpha = 1$. Curves show test reward versus log-scale learning rate $\log_2(\eta)$. Large markers indicate the optimal learning rate for each rank.

D.2. Case Study on the Relationship between Learning Rate and Training Time

In our experiment, we found that a suboptimal learning rate usually causes a longer training time under RLVR. We attribute this to a two-phase training pattern we find: in the first phase, the model explores the solution space by generating long sequences (often hitting the maximum generation limit); in the second phase, once the model learns to solve the task, it produces more concise solutions that are $4\text{--}5\times$ shorter. At near-optimal learning rates, the model quickly exits the exploratory phase, whereas at suboptimal rates it remains stuck and continues generating long sequences, prolonging each training step. Here, we conduct a case study examining this phenomenon. We compare FFT and $\text{Init}[\mathbf{B}]$ (with constant $\alpha = 1$ and rank $r = 256$) under two learning rate settings: the optimal rate ($\eta = 2^{-18}$) and a suboptimal rate ($\eta = 2^{-16}$).

As shown in Figures 15a and 15b, training and test rewards collapse to near zero under the suboptimal learning rate, whereas they steadily increase under the optimal rate. More importantly, with the optimal learning rate, the training exhibits the two-phase pattern discussed above: as shown in Figure 15c, completion lengths initially approach the maximum generation limit (1024 tokens) during early exploration (steps < 50), then sharply decrease to approximately 200 tokens (a $4\text{--}5\times$ reduction) around step 100 as the model learns to produce concise solutions. In contrast, models trained with the suboptimal learning rate remain stuck in the exploratory phase, consistently generating maximum-length completions throughout training. This directly translates to longer per-step training times, as shown in Figure 15d: models with optimal learning

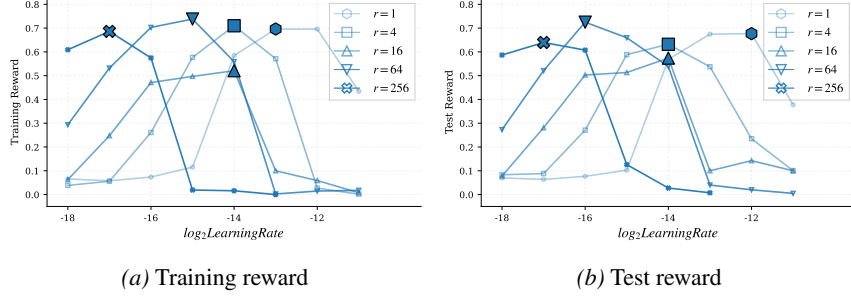


Figure 14. RLVR results on Llama-3.1-8B (GSM8k) for Init[A] with $\alpha = 1$. (a) Training reward and (b) test reward versus log-scale learning rate $\log_2(\eta)$. Large markers indicate the optimal learning rate for each rank.

rates require only 4–5 seconds per step, while those with suboptimal rates require 15–22 seconds—a 3–5× increase.

In Table 8, we sample responses from the model to a fixed question during full finetuning with optimal and suboptimal learning rates. With the optimal learning rate, the model first learns to follow the specified format, then attempts to solve the problem, and finally learns to simplify its solution. In contrast, with the suboptimal learning rate, the model fails to follow the specified response format at the beginning and eventually collapses into repetitive token generation.

We note one exception: Init[B] with $\alpha = 1$ and a higher learning rate ($\eta = 2^{-15}$) also exhibits shorter per-step training times. However, this represents the opposite failure mode—rather than remaining stuck at maximum-length generations, the model collapses and stops generation almost immediately, producing completions of ~ 2 tokens, as shown in Figure 16.

E. Additional Results for Text-to-Image Diffusion Model Finetuning

E.1. Learning Rate Sweep Results

Figure 17 shows learning rate sweeps for Init[A] with $\alpha = 1$. Consistent with our theoretical prediction that $\eta \propto r^{-1/2}$, the optimal learning rate η shifts left by approximately 1 on the \log_2 scale for every 4× increase in rank r .



Figure 15. Case study comparing optimal ($\eta = 2^{-18}$) and suboptimal ($\eta = 2^{-16}$) learning rates for FFT and Init[B] ($\alpha = 1$ and $r = 256$). (a) Training reward and (b) test reward show that suboptimal learning rates cause reward collapse, while optimal rates yield steady improvement. (c) Maximum completion length reveals the two-phase training pattern: under optimal learning rates, models transition from generating near-maximum-length sequences (~ 1024 tokens) to concise solutions (~ 200 tokens), whereas suboptimal rates cause models stuck in the exploratory phase with persistently long outputs. (d) Per-step training time directly reflects the completion length, with optimal learning rates achieving 3–5× faster for each training step.

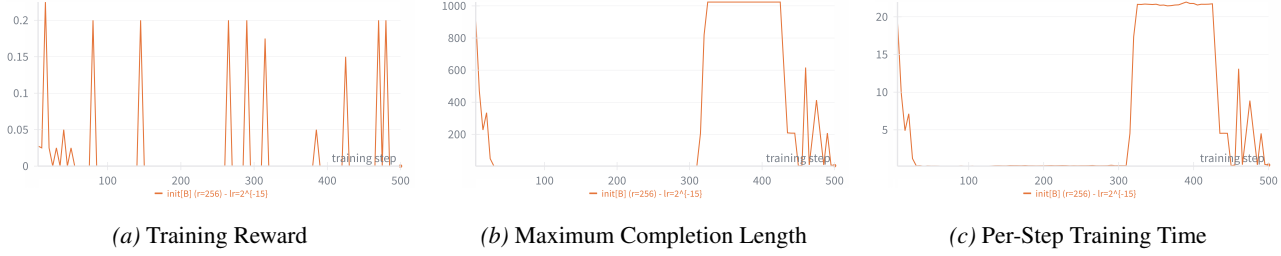


Figure 16. RLVR finetuning dynamics for Init[B] with rank $r = 256$ and learning rate $\eta = 2^{-15}$.

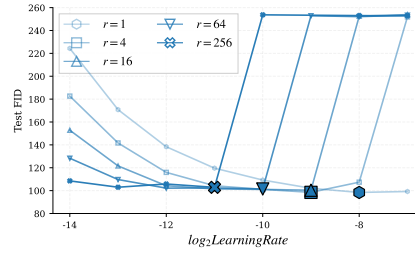


Figure 17. Results on Stable-Diffusion-1.5 (naruto-blip-captions). The figure plots validation FID score versus $\log_2(\eta)$ under Init[A] with $\alpha = 1$. Large markers denote the best learning rate for each curve.

Table 8. Generated responses to a selected question at different training steps for FFT with optimal (left column) and suboptimal (right column) learning rates. [...]truncated] indicates that part of the response has been shortened for brevity.

Question: Jerry is twice as old as he was 5 years ago. How old will Jerry be in 3 years?

Answer: 13